El Niño Modoki and its possible teleconnection

KARUMURI ASHOK, SWADHIN K. BEHERA, SURYACHANDRA A. RAO, HENGYI WENG

Frontier Research Center for Global Change/JAMSTEC, 3173-25, Showamachi, Kanazawa-Ku, Yokohama, Kanagawa, 236-0001, Japan

TOSHIO YAMAGATA

Frontier Research Center for Global Change/JAMSTEC, 3173-25, Showamachi, Kanazawa-Ku, Yokohama, Kanagawa, 236-000, Japan
and
Department of Earth and Planetary Science, Graduate School of Science, The University of Tokyo, Hongo 7-3-1, Bunkyo-ku, Tokyo 113-0033, Japan

---

Corresponding author address: Dr. Toshio Yamagata, Professor,
Department of Earth and Planetary Science, Graduate School of Science,
The University of Tokyo, Hongo 7-3-1, Bunkyo-ku, Tokyo 113-0033, Japan
Tel: 81-3-5841-4297; Fax: 81-3-5841-8791; Direct Tel and Fax: 81-3-5800-6942
E-mail: yamagata@eps.s.u-tokyo.ac.jp

ABSTRACT

Using observed datasets mainly for the period 1979-2005, we find that anomalous warming events different from conventional El Niño events occur in the central equatorial Pacific. This unique warming in the central equatorial Pacific associated with a horse-shoe pattern is flanked by a colder sea surface temperature anomaly (SSTA) on both sides along the equator. EOF analysis of monthly tropical Pacific SSTA shows that these events are represented by the second mode that explains 12% of the variance. Since a majority of such events are not part of El Niño evolution, the phenomenon is named as El Niño Modoki[1] (Pseudo-El Niño). The El Niño Modoki involves ocean-atmosphere coupled processes which include a unique tripolar sea level pressure pattern during the evolution, analogous to the Southern Oscillation in case of El Niño. Hence, the total entity is named as ENSO Modoki. The ENSO Modoki events significantly influence the temperature and precipitation over many parts of the globe. Depending on the season, the impacts over regions such as the Far East including Japan, New Zealand, western coast of USA etc. are opposite to those of the conventional ENSO. The difference maps between the two periods of 1979-2004 and 1958-1978 for various oceanic/atmospheric variables suggest that the recent weakening of equatorial easterlies related to weakened zonal sea surface temperature gradient led to more flattening of the thermocline. This appears to be a cause of more frequent and persistent occurrence of the ENSO Modoki event during recent decades.

[1] "Modoki" is a classical Japanese word, which means "a similar but different thing".

1. Introduction

From the point of climate variability, the year 2004 was very unusual. We start from mentioning some examples. During the summer of that year from June to September, southern India, along with some parts of northern India experienced droughts (Figure 1a). Parts of Japan as well as Korea also experienced severe drought and heat wave, while Philippine Islands received surplus rainfall. A large part of Australia experienced deficit in austral winter rainfall. Tasmania and New Zealand, on the other hand, received surplus precipitation. Southern Mexico and Ecuador regions suffered from drought, whereas Northern Brazil received surplus rainfall. We notice that sea surface temperature anomalies (SSTA) in the equatorial Pacific showed a peculiar zonal tripole pattern (Figure 1b): While the central tropical Pacific was warmer than normal, it was flanked by anomalously cooler SSTA to its east and west. This anomalous SSTA pattern is different from that during typical El Niño events [e.g. *Rasmusson and Carpenter*, 1982]. The condition continued through the following boreal winter (figure not shown).

In 2003, the National Oceanic and Atmospheric Administration of the United States of America (NOAA) revised[2] the definition of El Niño "as a phenomenon in the equatorial Pacific Ocean characterized by a positive sea surface temperature departure from normal (for the 1971-2000 base period) in the Niño 3.4 region (See Table 1 for definition) greater than or equal in magnitude to 0.5^{o}C, averaged over three consecutive months". *Larkin and Harrison* [2005] refer to this redefined El Niño as "Dateline El Niño", and mention that the warming may not reach NINO3 region during Dateline El Niño events. Interestingly, the 2004 event is not exactly covered by this definition

2 Details can be found at http://www.noaanews.noaa.gov/stories/s2095.htm. The definition has been adopted by the World Meteorological region IV [*Larkin and Harrison*, 2005].

because the warmer central region extends from the western fringe of the NINO4 region rather than being just confined to the NINO3.4 region (Figure 1b). Moreover, the western Pacific and eastern Pacific SST anomalies during the boreal summer of 2004 were significantly colder than normal [*Ashok et al.*, 2007b; available at http://www.jamstec.go.jp/frsgc/research/d1/iod/]. In particular, the magnitude of the cooler than normal SSTA in the eastern tropical Pacific is comparable to that of the warmer central pole. Given the maximum boreal summer warming in central tropical Pacific distinctly persisted through the following boreal winter [*Ashok et al.,* 2007b], it is not surprising that experts have started debating on whether to classify that year as an El Niño year [*World Meteorological Organizati*on, 2005]. The peculiarity of events such as the 2004 event was also noticed by *Donguy and Dessier* [1983] and *Meyers et al.* [2007]. In fact, hints for existence of the interesting SSTA pattern in the tropical Pacific that is different from ENSO are also found in earlier works such as *Weare et al.* [1976] and *Meyers et al.* [1999].

Because of the obvious distinction from the traditional El Niño [*Rasmusson and Carpenter*, 1982] and even from that defined by NOAA in 2003, we refer to the SSTA pattern observed in 2004, namely, warming in the central Pacific (~NINO4 region) flanked by colder SSTA to the west and east, as an El Niño Modoki[3] (Pseudo-El Niño)

3 This word was introduced by one of the present authors T. Yamagata during 2004 while explaining a probable cause behind the abnormal summer climatic conditions over Japan. It has been often used since then by various Japanese Mass Media. "Modoki" is a classical Japanese word which means "similar but different". A news also appeared in "Japan times" on July 24, 2004 under the heading "'Mock El Nino' culprit behind heat wave, floods: Professor", which follows: "The heat wave and floods in various parts of Japan are being caused by an El Nino-like phenomenon in the central Pacific Ocean, a Japanese researcher said Friday. Toshio Yamagata, a professor at the University of Tokyo specializing in climate dynamics, said an increase in the sea surface temperature has activated convection currents and promoted a high-pressure ridge in the Pacific, bringing a hot summer to Japan ……." For further details of this news, see http://www.japantimes.co.jp/cgi-bin/getarticle.pl5?nn20040724f3.htm
Some other links to Japanese news items and related articles follow:

event; this term is now popular in Japan and East Asia. We believe that identifying a unique phenomenon with the most appropriate definition, just as new species in biology, is important to promote further research. This is a key issue of the present study.

This paper is composed of four sections. The datasets and methods of analysis are briefly described in section 2. Section 3 discusses the analyzed results, where we justify the reason for classifying the phenomenon in 2004 and other similar ones as an entity different from the conventional El Niño and even the so-called dateline El Niño. The possible teleconnections of the typical SSTA pattern associated with the El Niño Modoki (Pseudo- El Niño) are identified, along with a discussion on the mechanism for formation of the unique SSTA pattern and that for teleconnections. This further verifies the novel aspect of the present research. Section 4 is reserved for discussion on why such an event as in 2004 occurs more frequently since the late 1970s and suggests a possible link with the recent global warming. The summary and concluding remarks are presented in section 5.

2. Datasets and methods of analysis

The Hadley Centre Global Sea Ice and Sea Surface Temperature (HadISST) Analyses datasets [*Rayner et al.,* 2003] from January1958 to February 2005 are used in this study. For verification, we also use the Optimally Interpolated Sea Surface Temeprature (OISST) datasets [*Reynolds,* 2002] for the period from January 1982 through March 2005. For precipitation analysis, we mainly use the Version 2 Global Precipitation Climatology Project (GPCP) Monthly Precipitation Analysis [see *Adler et*

---

http://www.kyoto-np.co.jp/kp/special/ecology/eco/eco63.html
http://www.tbs.co.jp/morita/qa_nanmon/faq_040811-1.html

al., 2003 and references therein] for the period from 1979 through 2004. The results are verified by the use of Climate Prediction Center Merged Analysis of Precipitation (CMAP) data [*Xie and Arkin*, 1996] for the same period; unless specifically mentioned, all the discussion in this study related to precipitation analysis is based on GPCP datasets. The NCEP/NCAR reanalysis products [*Kalnay et al.*, 1996] such as the sea level pressure, geopotential, and wind datasets from 1958 through 2005 are also employed in this study. We also use the surface wind datasets from ECMWF reanalysis [ERA 40; *Simmons and Gibson*, 2000] available from January 1958 till August 2002 for verification of decadal trends in low level equatorial zonal winds over the tropical Pacific. The recent ocean heat content datasets for the upper ocean down to 300 m depth [*Levitus et al.*, 2005] are used to assess the long-term changes. We also utilize the Sea Surface Height (SSH) data derived from Simple Ocean Data Assimilation (SODA) product for the period from 1979 through 2004 [*Carton et al.*, 2005; *Carton and Giese*, 2007].

The present analysis covers basically the ocean and atmospheric data from January 1979 to February 2005 (December 2004 for GPCP and CMAP datasets), unless specified otherwise. Anomalies are deviations from climatology in the above base period. The reason choosing the post-1978 data is twofold. The first is availability of better and more reliable data quality, particularly in National Centers for Environmental Prediction/National Center for Atmospheric Research global reanalysis data [NCEP/NCAR; *Kalnay et al.*, 1996] dataset over the Southern Hemisphere [see Kistler et al., 2001; Trenberth et al., 2001 for details]; also, some of the datasets such as the CMAP data [*Xie and Arkin*, 1996] are only available from 1979. The second is that by using

datasets from 1979, we avoid necessity of stratifying events before and after the Pacific regime shift [see *Nitta and Yamada*, 1989; *Stephens et al.*, 2001; *Deser et al.*, 2002; *Hartman and Wendler*, 2005 for details and further references] that occurred around the middle of 1970s.

Further, we use the NCEP/NCAR 2m temperature datasets to examine the potential impacts of the El Niño Modoki. As the reanalysis for this parameter is to some extent dependent on model parameterizations used in the reanalysis, we have also analyzed the observed Climate Research Unit (CRUTEM3) monthly land surface temperature [*Jones et al.,* 1996] available at 5ºX5º for the period 1979-2004 to validate the NCEP/NCAR 2m temperature datasets.

We first carry out an Empirical Orthogonal Function (EOF) analysis, using singular value decomposition (SVD), on SSTA to identify modes of variability relevant to the El Niño Modoki (Pseudo-El Niño) pattern as observed in summer of 2004; the dominant two patterns obtained from the EOF analysis are confirmed by a complex EOF analysis (see Appendix I). We then try to extract the apparent teleconnection patterns using partial correlation technique (see Appendix II for details) and composite analysis. Each of the monthly indices and anomaly fields have been seasonally averaged over a period from June to September, and December to February to obtain what we hereafter refer to as the boreal summer and winter values, respectively. The significance levels for composite and partial correlation analyses were obtained by the standard 2-tailed Student's t-test; we have further verified the significant correlation zones by employing a Monte Carlo method with 1000 simulations (see Appendix II).

3. Variability related to El Niño Modoki

a. Climate modes of the tropical Pacific variability

The first four leading EOF modes of the monthly SSTA over the tropical Pacific region are presented in Figure 2. The EOF1 pattern shown in Figure 2a captures the well-known El Niño pattern [*Rasmusson and Carpenter*, 1982]. This mode explains about 45% of the tropical Pacific SST variability for the period between 1979 and 2004. The EOF2 that explains 12% of the SST variability captures a zonal tripole pattern in the tropical region (Figure 2b). Both eastern and western tropical Pacific SSTAs have loadings of the same sign, while those of the central tropical Pacific are opposite. In higher latitudes, the positive loadings in the central equatorial Pacific spread eastward in both hemispheres, and this horse-shoe pattern straddles the tongue of negative loadings in the equatorial eastern Pacific. The magnitudes of the loadings in the central and eastern Pacific are comparable. The SSTA for the summer of 2004 shown in Figure1b is similar to this EOF2 pattern. In particular, the SSTA pattern continued till the end of boreal winter in 2004. There are several other years such as 1980, 1986, 1990, 1991, 1994, 2002 when an anomaly pattern similar to that in Figure 2b (and Figure 1b) is observed. As the variances explained by the first two EOF patterns are well separated [*North et al.*, 1982] and are supported by the results from the complex EOF analysis discussed later in this section as well as in the Appendix I, it is reasonable to expect that these two patterns represent different modes of climate variability. Therefore, we refer to the EOF2 SSTA pattern associated with the positive phase of its principal component (Figure 3) as an El Niño Modoki (Pseudo-El Niño) event. Consequently, in analogy with the nomenclature

of El Niño events, we refer to a reversed event such as in 1998 with the anomalously cold SSTA in the central equatorial and subtropical Pacific flanked by the warmer than normal SSTA on both sides along the equator (figure not shown) as an La Niña Modoki (Pseudo-La Niña) event.

The EOF3[4] and EOF4 patterns (Figures 1c and 1d) explain only about 7% and 4.6% of the variance respectively. We repeated the EOF analysis with the OISST [*Reynolds,* 2002] datasets from 1982 through 2005, and the results are well in agreement with the afore-mentioned findings. The robustness of the EOF patterns was also examined by confining the meridional domain to 10ºS-10ºN (figures not shown); the EOF2 pattern in the tropics and the associated tropical Pacific SSTA variance do not change significantly even for the meridional domain expanded to 45ºS-45ºN (figure not shown). The tripolar structure of the second mode of tropical Pacific SSTA variability was also verified by Varimax rotation of first 10 EOF modes (figures not shown). Further, from the tropical SSTA, we removed the reconstructed EOF1 component that was obtained by multiplying the EOF1 loadings (Figure 2a) with the associated PC1. An EOF analysis of the remainder indicates that the EOF1 and its principal component obtained from this exercise strongly resemble (Figures not shown) those of the EOF2 of the total SSTA shown in Figure 2a. The variance explained by this El Niño Modoki-associated mode increases to 21% in the absence of ENSO-related EOF1 signal. This exercise further demonstrates the robustness of the EOF2 mode, and indicates that El Niño Modoki may be independent of the ENSO signal.

[4] The results from a similar EOF analysis of the *linearly detrended* tropical SST datasets (Figures not shown) do not change the properties of the top two modes much, except that the variance explained by the EOF1 rises to 47%. However, the present EOF3 disappears completely, indicating that the EOF3 is nothing but the background trend.

We also carried out a complex EOF (CEOF) analysis on the tropical Pacific SSTA and SODA sea surface height anomalies (SSHA) to get the propagation characteristics of these events. The real component of the complex EOF1 and EOF2 are similar to those shown in Figures 2a and 2b (figures not shown). The phase diagram of the CEOF1 (Figure A1-1 shown in Appendix I) demonstrates that the phase of the CEOF1 propagates mainly from west to east prominently in the equatorial regions confirming the importance of oceanic Kelvin waves for El Niño. Unlike the phase of first CEOF mode of SSH, phase for the second mode propagates from east to west in the off-equatorial regions and west to east in the central equatorial Pacific, suggesting that the off-equatorial Rossby waves and equatorial Kelvin waves are involved in the formation of El Niño Modoki event; this distinct aspect will be discussed further in subsection 2c. The amplitudes of the complex EOF are provided in Figures A1-2.

The time series of the normalized principal components (PCs) of EOF1, EOF2, and EOF3 are presented in Figure 3. The correlation between PC1 and PC2 is zero by definition. A cross-correlation analysis between PC1 and PC2 at different leads and lags gives a maximum correlation of 0.43 with PC2 leading PC1, indicating that substantial percentages of the variances explained by the EOF2 and EOF1 are not explained by each other during the study period.

The correlation between PC1 and NINO3 index is very high, and amounts to 0.98, which proves that EOF1 represents the conventional El Niño well. On the other hand, the correlation between PC2 and NINO3 index is very low (-0.09). All these prove that the El Niño Modoki events are not related to the conventional El Niño events. *The El Niño Modoki needs to be addressed as a unique phenomenon in the tropical Pacific.* The

correlation between the NINO4 index and PC2 is 0.51. This significant correlation is expected to some extent because the central pole of the EOF2 is located around the NINO4 region. The correlation between the NINO3 and NINO4 indices is 0.73. Since the NINO4 SST index is related to both indices of the El Niño and El Niño Modoki, we need to be careful when we use the NINO4 index as a conventional ENSO index, at least after 1978. The correlation between NINO1+2 index and PC2 is 0.44. The correlation between NINO3.4 index and the PC2 is 0.19, which is rather small; this demonstrates that the El Niño Modoki events are different even from the so-called "Dateline ENSO" events. The correlation of the PC2 with the Indian Ocean Dipole Mode Index [*Saji et al.*, 1999] and the Subtropical Dipole Mode Index [*Behera and Yamagata*, 2001] are only 0.1 and 0.15, respectively.

Based on the EOF2 pattern presented in Figure 2b and the PC2 time series shown in Figure 3, we derive an El Niño Modoki index (EMI). Because of the unique tripolar nature of the SSTA, the index is defined as follows:

$$EMI = [SSTA]_A - 0.5*[SSTA]_B - 0.5*[SSTA]_C \quad \text{……..(1)}$$

The square bracket in Equation (1) represents the area-averaged SSTA over each of the regions A (165^{o}E-140^{o}W, 10^{o}S-10^{o}N), B (110^{o}W-70^{o}W, 15^{o}S-5^{o}N), and C (125^{o}E-145^{o}E, 10^{o}S-20^{o}N), respectively. The time series of the EMI is shown in Figure 4a. The correlation between this new time series and the PC2 is 0.91, which is statistically significant at a 99% confidence level from a 2-tailed Student's t-test. This strong correlation shows that the index introduced here is appropriate to represent the El Niño Modoki events of the tropical Pacific. To examine its relationship with other indices in

the tropical and subtropical Indo-Pacific regions, various correlation values are shown in Table 2.

Trenberth and Stepaniak [2001] introduced another index called Trans-Nino index (TNI) as the difference between normalized SSTA between NINO4 and NINO1+2. TNI is correlated at 0.8 with the time series of SVD2 of SSTA and several atmospheric fields such as precipitation [*Trenberth et al.*, 2002], and hence they accept TNI as an index (see Figure 4b) to represent the SVD2 in tropical Pacific; the correlation of the SVD2 time series with tropical Pacific SSTA resembles that of our EOF2 shown in Figure 2. The correlation between TNI and EMI is -0.87 for the study period. From this simple analysis, TNI appears to be almost the same with EMI. Nevertheless, we will show the advantage of EMI in the following. The correlations of the PC2 with NINO4 and NINO1+2 indices are 0.51 and -0.44 respectively. On the other hand, its correlations with SSTA in our equivalent boxes A and B (see equation 1) in the central and eastern tropical Pacific are 0.51 and -0.42. Up to that, both indices are similar. However, the correlation of the PC2 with our western box (Box C defined in equation 1) is -0.453, stronger in amplitude than that with NINO1+2, the eastern box of SSTA defining the TNI. This demonstrates that the western tropical Pacific SSTA is just as important as that of the eastern Pacific; this important aspect must be taken in to account in introducing a new index capturing the EOF2 type of phenomena in the tropical Pacific. Although the variances of SSTA contributing to the EOF2 in the tropical western Pacific are weaker than those in the tropical eastern Pacific, they are important because events such as 2004 are triggered in the western tropical Pacific [see *Ashok et al.*, 2007b]; this aspect is important for predicting the El Niño Modoki**,** and will be discussed in detail in subsection

'c' of this section. Because of this importance of the western tropical Pacific, it is also worth noticing that the correlation of the western tropical Pacific SSTA with EMI is -0.51, much higher in magnitude than the correlation of 0.25 with TNI. From all the above, the EMI seems to be, statistically as well as dynamically, a better index for capturing the EOF2 pattern of tropical Pacific SSTA variability. The relative correlations of EMI and TNI with PC2 are 0.93 and 0.88, elucidating the slight superiority of EMI. However, because of their strong similarity and association with EOF2, both indices may be considered analogous in representation of the El Niño Modoki for many practical purposes, just as the NINO3 and NINO3.4 indices in case of El Niño events.

Trenberth and Stepaniak [2001] and *Trenberth et al.* [2002a,b] suggest that SSTA of the TNI type is only one aspect of ENSO evolution. In the next section, we will demonstrate that this is unfortunately not correct for a majority of the events during the study period. This is the major difference between the present study and the important preceding work by *Trenberth and Stepaniak* [2001], and makes the present research unique.

The correlation between the principal component of the EOF3 and EMI for the study period is only 0.24, indicating that EOF3 is not related El Niño Modoki. But, its potential role will be further examined in section 4.

b. A composite picture of El Niño Modoki

Based on the time series of the EMI shown in Figure 4a, we have identified seven typical[5] El Niño Modoki events that lasted from boreal summer through boreal winter,

[5] We call an El Niño Modoki event "typical" when its amplitude of the index is equal to or greater than 0.7σ, where σ is the seasonal standard deviation.

peaking in one of these seasons (seasonal standard deviations for boreal summer and winter are 0.5ºC and 0.54ºC respectively). These typical El Niño Modoki events occurred in 1986, 1990, 1991, 1992, 1994, 2002, and 2004. Additionally, we identified a typical El Niño Modoki during the boreal winter of 1979-80 that lasted through the summer of 1980, though its amplitude fell below the threshold of 0.7σ by then. The SSTA patterns in these seven boreal summer seasons, and eight winter seasons including 1979-80, have been composited for a common picture by removing high-frequency noise. The result is remarkable and shown in Figure 5a and 5b respectively.

During the boreal summer when an El Niño Modoki event occurs, the significantly warmer SSTA in the central equatorial Pacific is flanked by significantly colder-than-normal SSTA in the western and eastern tropical Pacific. This composite pattern for summer captures the EOF2 pattern presented earlier in Figure 2b quite well.

The El Niño Modoki occurs not only in boreal summer months but also in boreal winter months from December to February (DJF). Figure 5b shows the composite SSTA in the boreal winter months. The composite pattern is qualitatively similar to that in summer (Figure 5a) and EOF2 (Figure 2b). The colder SSTA is relatively more widespread in the western tropical Pacific as compared to that in the eastern Pacific during boreal winter, whereas it is the other way round during boreal summer. The colder SSTA during boreal winter in the eastern tropical Pacific shifts southward due to spread of warmer anomalies from the central Pacific. We also note that El Niño Modoki events persisted from 1990 through 1994 with changing amplitude. The phenomenon was discussed previously as either protracted or prolonged El Niño in the literature [cf. *Allan et al.*, 2003].

It is very interesting to note that during the El Niño Modoki events, the warmest SSTA does not propagate into the NINO1+2 region as they do during the conventional El Niño years such as 1987 and 1997 after the regime shift in the middle of 1970s [see discussion related to Figure 5; *Tozuka and Yamagata*, 2003; also *Ashok et al.*, 2007b]. Despite having identified the 2002 event in the tropical Pacific as a moderate El Niño event, *McPhaden* [2004] also noted this aspect as in the following. "The pattern of SST anomalies was unusual, however, with the largest anomalies concentrated in the central equatorial Pacific in contrast to the relatively weak and short-lived warming in the eastern Pacific and along the west coasts of the Americas. Precisely what accounted for this SST anomaly pattern is unclear". *McPhaden* [2004] also noticed, in agreement with the present work, that the spatial pattern of the SSTA resembled that during 1994/95 but contrasted with 1997 El Niño; he also discussed the unique teleconnections during 2002.

Trenberth and Stepaniak [2001] indicate that NINO3.4 and TNI are significantly correlated at different lags/leads, and hence they conclude that their SVD2 pattern is one phase of ENSO evolution. However, they admit that the relationship has changed along with changes in ENSO characteristics after the climate regime shift in the middle 1970s [*Nitta and Yamada*, 1989; *Stephens et al.*, 2001, *Deser et al.*, 2002; *Hartman and Wendler*, 2005]. It is seen in the Figure 2 of *Trenberth and Stepaniak* [2001] that the lag/lead moving correlations have considerably weakened after 1976; these also changed their respective signs. Hence, their conjecture that the El Niño Modoki pattern of SSTA is part of El Niño evolution [*Trenberth and Stepaniak*, 2001; *Trenberth et al.*, 2002] is not always supported. For example, *Ashok et al.* [2007b] bring out distinctness of the 2004 El Niño Modoki event and point out that it cannot be described as part of the ENSO

evolution. According to this study, it can be seen that, the time series of principal component of EOF2 as well as EMI are positive most of the time after March 2002 (also see Figure 4a). On the other hand, the time series of the NINO3 and NINO3.4 indices change their phase several times, and their amplitude is weak after 2002 [figures not shown; see Figure 4 of *Ashok et al.,* 2007b]. Even during 2002, however, the EOF2 was dominant as compared to EOF1, as evidenced by the time series of the principal components (Figure 4a). Besides, the SSTA in the NINO4 region during this period was consistently warm [figure not shown; see Figure 2 of *Ashok et al.*, 2007b], indicating that the tropical Pacific was continuously in the positive phase of quasi-EOF2 mode condition since spring of 2002. If the hypothesis of *Trenberth and Stepaniak* [2001] applies, the El Niño Modoki conditions in summer of 2004 should have been followed (preceded) by an El Niño (a La Niña) after (before) 3-12 months; neither of these things happened, as indicated by the NINO3.4 index shown in Figure 4 or by the NINO3 index [see Figure 4 of *Ashok et al., 2007b*]. In fact, out of the three major El Niño events after 1977, only the 1982-83 period fits the hypothesis stipulated by *Trenberth and Stepaniak* [2001]. Even during 1997 when a strong El Niño event occurred, it was preceded by a very weak El Niño Modoki event (see Figure 4b). Importantly, it can also be seen from Figure 4b that the condition suggested by *Trenberth and Stepaniak* [2001] is not valid for the so-called protracted El Niño period of 1990-94.

To further understand the relationship between El Niño Modoki and El Niño, a lead-lag analysis between the monthly values of the EMI and NINO3 index was carried out for the study period. It has turned out that EMI in April (October) is correlated at about 0.55 (0.45) with NINO3 index in December. On the other hand, February NINO3

index leads the August EMI with correlation of about 0.5. Similarly, Nino 3.4 index shows maximum correlation of 0.49 with EMI at 4 months lag. All these indicate that, after 1978, *only up to a maximum of* 30% of the total variance of either one of the El Niño Modoki and El Niño phenomena can be explained by the other. The analysis in this subsection clearly brings out the uniqueness of the El Niño Modoki events, and shows that they cannot be described as part of the El Niño evolution.

c. Coupled processes of ENSO Modoki events

In this section, we discuss possible mechanisms for the evolution of the El Niño Modoki. To visualize the ocean-atmospheric coupled nature of the El Niño Modoki, we carry out lag/lead correlation analyses between EMI with various variables such as SSHA, wind stress anomalies, sea surface pressure anomalies, and ocean temperature anomalies at 10 m depth (T_{10}) from the SODA datasets [*Carton and Geise*, 2005, *Carton et al.*, 2005]; The near-surface temperature data of OISST [*Reynolds*, 2002] were used in the SODA dataset version 1.4.3 to update the mixed-layer temperature, and hence the impact from the heat flux boundary condition, provided by a bulk formula, is relatively unimportant [*Carton and Giese*, 2007]. Relatively high correlations between EMI and SSH anomalies are seen in the central and western tropical Pacific even at 12 months lag with the EMI lagging SSHA (Figure 6a). Positive (negative) correlation coefficients are observed in the central (western) Pacific. Coinciding with those, we also observe positive (negative) correlation coefficients for T_{10}. This appears to be excited by westerly wind anomalies in the western Pacific because those westerly wind anomalies, by transporting the warm water in the off-equatorial western Pacific to the equator, may

drive downwelling equatorial Kelvin waves and induce deepening of the thermocline from the central to eastern Pacific. The wind anomalies are consistent with the surface pressure anomalies as seen in Figure 7a, b.

In the following months, positive correlations with SSH anomalies become higher and propagate westward together with correlations of T_{10}. At 6 months lag, we observe easterly wind anomalies in the eastern Pacific in addition to the anomalous westerlies in the western Pacific (Figure 6c). Since these winds cause convergence in the central Pacific, the thermocline in central Pacific further deepens. With increasing easterlies in the eastern Pacific, the equatorial Rossby waves may deepen the thermocline off the equator and thus increase the warming in the central Pacific as indicated by the high correlations in the central Pacific at zero lag (Figure 6e). The evolution of the surface pressure anomalies is consistent again with the wind evolution (Figure 7c-e). The vertical distribution of lag correlations between subsurface temperature anomalies averaged between 4ºS and 2ºS and EMI confirms the above picture (Figure 8). The warming in the central Pacific is thus strengthened owing to the arrival of downwelling equatorial Kelvin waves from the west and Rossby waves from the east. Highest correlations, in general, are found at subsurface depths at zero lag (Figure 8e) as in other near-equatorial latitudes (6ºS-4ºS, 2ºN-4ºN, 4ºN-6ºN, figures not shown), indicating that the SST warming in the central equatorial Pacific is due to those subsurface oceanic processes.

After the peak of El Niño Modoki, anomalous easterlies in the eastern Pacific are further strengthened, and the equatorial upwelling is strengthened. The excited downwelling Rossby waves propagate further west and, together with the weakening

westerlies in the western Pacific, smear out the cold anomaly in the western Pacific. Thus the Modoki phenomenon is terminated (Figures 6f-j,7f-j, 8f-j,).

The above picture demonstrates that the evolution of El Niño Modoki involves ocean-atmosphere coupled processes. Further, Figures 6-8 show a link of the El Niño Modoki with a distinct atmospheric component; the situation is analogous to the association of El Niño with the Southern Oscillation [*Bjerknes*, 1969; *Philander*, 1990]. Also, we have derived an atmospheric index by replacing SSTA in the equation 1 with sea level pressure anomalies (SLPA), and reversed its sign (figure not shown). This atmospheric index has a significant correlation of 0.7 with EMI, demonstrating that there is a strong atmospheric response associated with the El Niño Modoki events. Thus, the total entity should be referred to as ENSO Modoki.

The tropical central Pacific is the common playground for both ENSO and ENSO Modoki. This is reflected in the lead/lag correlations between the indices of these phenomena, as discussed in subsection 3a. It is important, however, to notice that the magnitude of these correlations is relatively modest. During the prominent El Niño events in years such as 1982-83 and 1997-98, the central Pacific warming propagates to the eastern Pacific. However, during majority of the El Niño Modoki events, the propagation takes place only up to the central Pacific.

It is also important to notice that the ENSO Modoki time scales are different from ENSO. Based on a wavelet power spectrum analysis, we find (figure not shown), at a 90% significance level above red noise, (i) an interannual signal with 4-year periodicity and (ii) a slowly varying signal with a 12-year time scale. The strong decadal signal modulating the interannual signal of EMI can be seen in Figure 4a. This strong decadal

signature is unique to the EMI in the tropical Pacific; a similar wavelet power spectrum for NINO3 index for the period 1979-2004 does not exhibit any decadal peak significant at a 90% level above red noise. We note that the maximum monthly lead/lag correlations between the EMI and an index of the Pacific Decadal Oscillation [*Zhang,* 1997; *Mantua et al.,* 1997] is about 0.4, indicating that a maximum of about 16% variance of either one of these phenomena is related to the other.

The coupled processes discussed in this subsection apparently play a major role in setting up the interannual variability of the ENSO Modoki phenomenon. Further differences between the time scales of ENSO and ENSO Modoki are discussed in *Weng et al.* [2007].

Preliminary examination of the lead/lag correlations of the SSHA with the statistically significant decadal signal of EMI indicates some weak and slow wave propagation in the tropical and subtropical Pacific (figures not shown); this apparent propagation is different from that of similar correlations between the SSHA and the decadal signal of NINO3 SSTA, with the ENSO Modoki (ENSO) signal persisting largely in the tropical central (eastern) Pacific. However, this slow propagation may due to a statistical artifact. As our data span is only for 26 years, any interpretation of the decadal changes based on filtering has to be done with caution. The identification of a possible mechanism for the decadal variability of this phenomenon needs analyses of results from a high-resolution coupled model. This will be topic for future research.

d. Potential impacts of the ENSO Modoki

It is known that ENSO and IOD generate atmospheric changes globally through teleconnections [*Ropelewski and Halpert,* 1987; *Aceituno,* 1988; *Trenberth et al.*, 1998; *Diaz et al.*, 2001; *Saji and Yamagata*, 2003; *Yamagata et al.*, 2004 for more details and further references]. For example, *Navarra et al.* [1999] tried to identify impacts of changes in the location of boreal summer peak warming in the tropical Pacific on the Indian summer monsoon. *Kidson et al.* [2002] discussed the different impacts of "Moderate" and "Strong" El Niños; their analyses, however, do not highlight the uniqueness of strong El Niño Modoki events. *Larkin and Harrison* [2005a,b] have recently tried to study the autumn and winter impacts of the so-called "dateline" El Niño by composite analysis. Since their index is based on NINO3.4, their selection of years does not cover El Niño Modoki years 1979/80, 1991, 1992 and 2002 (and also 2004, because their study is for the period 1950-2003).

As the ENSO Modoki is associated with significant seasonal changes in the tropical SST and surface pressure changes, it is beneficial to study its potential impacts on the global climate by introducing seasonal stratification.

1) Boreal summer season

Figure 9a shows the composite GPCP [*Adler et al.,* 2003] rainfall anomalies in the JJAS season of the seven positive El Niño Modoki years 1986, 1990, 1991, 1992, 1994, 2002, and 2004. Statistically significant surplus rainfall anomalies are seen in the central equatorial Pacific region flanked on both sides by the negative rainfall anomalies in the equatorial western and eastern Pacific. The atmospheric condition associated with

the western pole located in the equatorial western Pacific apparently influences maritime countries such as Indonesia, Malaysia, Singapore etc, and the apparent teleconnection extends northwest up to south India and also Sri Lanka. The teleconnection associated with the positive rainfall anomaly in the central pole (equatorial central Pacific) seems to extend westward via the Philippines, Myanmar to northern India. In the East Asian region, southern Japan suffers droughts during these years owing to the Pacific-Japan pattern [cf. *Nitta*, 1987]. The deficit rainfall in the western Pacific region is seen to extend southward to southeastern Australia, influencing a significant part of eastern Australia. The negative rainfall anomalies over the equatorial eastern Pacific extend over western coast of North America.

We adopt the partial correlation technique [e.g. *Pedhazur,* 1997; *Spiegel,* 1997; *Ashok et al.* 2007a] to isolate global impacts of the El Niño Modoki statistically from those of the ENSO and IOD during different seasons. ; this technique is equivalent to multiple regression (see Appendix II for details) In accord to the rationale of introducing the El Niño Modoki, the simultaneous linear correlation between the NINO3 index and EMI is very weak. Therefore, the partial correlations of the EMI with seasonal rainfall and temperature anomalies are not influenced in almost all regions by the correlations with the NINO3 index (figures not shown). The correlation between the IODMI and EMI is also weak as we have already shown. However, during some years such as 1994, El Niño Modoki and positive IOD occur simultaneously and influence each other. The partial correlations of the EMI with the JJAS rainfall anomalies over the period 1979-2004, after removing the linear influence of NINO3 index and the IODMI, are shown in Figure 9b. The result is similar to that in Figure 9a. However, Figure 9b demonstrates the

extensive influence of the ENSO Modoki on the eastern Australian region more clearly. The positive correlations from the central equatorial Pacific extend southeastward to southern regions of South America, indicating more than normal rainfall. The remarkable negative correlations in the eastern Pacific extend to the west coast of North America. This shows a dramatic contrast to the well-known impact of El Niño and is supported by an analysis using observed station data [*Weng et al.,* 2007]. We note that the negative correlations are also seen near Japan and south India. The robustness of the correlations has been reconfirmed by computing the significance levels based on a Monte Carlo method (Figure A2-1 in auxiliary information).

It is expected that the impact of La Niña Modoki, with cooling in the central Pacific flanked by warmer SSTA in eastern and Western tropical Pacific, may be opposite to that of El Niño Modoki [*Diaz et al.*, 2001].

Results obtained by repeating the composite analysis shown in Figure 9a with rainfall anomalies from CMAP datasets [*Xie and Arkin*, 1996] are qualitatively similar (figure not shown), though the magnitude of the significant composite anomalies is slightly different owing to the differences in the datasets (*Yin et al.,* 2004, and the references therein). This exercise demonstrates the robustness of our results. Hereafter, all the subsequent precipitation analyses will be only based on the GPCP datasets.

For comparison of the distinct impacts, the JJAS partial correlations between the NINO3 index and the rainfall anomalies over the period 1979-2004, with assuming the EMI and the IODMI as additional variables whose impacts have been removed, are presented in Figure 9c. In general, the results are in agreement with earlier studies [see *Diaz et al.*, 2001; *Saji and Yamagata*, 2003 for details and further references]. The

eastern tropical Pacific receives surplus rainfall during El Niño years, with deficit rainfall in the tropical western Pacific and the equatorial South America. In contrast to the El Niño Modoki summers, northwestern America receives surplus rainfall. Over much of the South American continent from equator to 40ºS, the impacts of ENSO and those of ENSO Modoki are opposite. The impacts of ENSO on Australian winter rainfall have changed over the decades as found out by *Meyers et al.* [2007]. The El Niño events are apparently only associated with surplus rainfall in central western Australia during the study period. The impacts of the IOD on boreal summer rainfall derived by partial correlation analysis are presented in Figure 9d. In general, the impacts are similar to those shown in earlier studies [see *Saji and Yamagata*, 2003; *Ashok et al.,* 2003; *Yamagata et al.*, 2004; *Behera et al.*, 2005; *Rao and Behera*, 2005]. Positive IOD events cause anomalously deficit rainfall in Indonesia, more than two-thirds of Australia, northern New Zealand, subtropical South America, parts of Mexico, North America, whereas surplus rainfall is seen in the region near the western pole of the IOD, Madagascar, parts of Africa etc. The correlation is largely positive in northern India, though it falls just below the statistically significance level in the present analysis. This is in agreement with earlier studies showing IOD impacts on the Indian monsoon region [*Ashok et al*., 2001; *Saji and Yamagata*, 2003; *Ashok et al.*, 2004]. Incidentally, we have repeated the multivariate analysis to assess the impacts of the IOD, ENSO, and ENSO Modoki by replacing the indices derived from HadISST with those from OISST for the available period (figures not shown). The correlations are qualitatively similar to those shown in Figures 9-11. However, with OISST indices, the positive (negative) correlations between the IODMI (NINO3 SSTA) and JJAS rainfall anomalies become statistically

significant at 90% confidence level from a 2-tailed Student's t-test over a wide region of monsoon trough over India. Similarly the negative IODMI-rainfall correlations become statistically significant over central Japan and Pakistan when we use the OISST datasets. However, even with Reynolds SST data, the impact of ENSO events on India is seen to be limited and confined to eastern central India. In comparison, the impact from ENSO Modoki is seen over a larger area in southern India.

In accord with the EOF analysis and composites of El Niño Modoki events, we find significant positive partial correlations between EMI and the surface air temperature anomalies over the central equatorial Pacific during boreal summer (Figure 10a). This positive correlation region apparently extends southeast; the positive correlations over Argentina and southern Brazil are significant, indicating that those regions experience warmer than normal winter during the El Niño Modoki event. Up north, significant cooling can be seen over northern Brazil, Columbia, and Venezuela, and parts of Mexico. Central and northern North America may also experience cooler summer during the El Niño Modoki years. Cooler than normal temperatures are also found around the maritime continent, in the tropical western Pacific, and in the southern part of China. These significant negative partial correlations extend to western and northern Australia and New Zealand. Many of the regions along the east coast of Africa may experience anomalously cooler boreal summers during the positive El Niño Modoki events. A wide region in West Asia covering countries such as Turkmenistan, and Kazakhstan, Armenia, Georgia etc. may also experience cooler than normal summer.

To validate the NCEP/NCAR 2m temperature datasets used in the above analysis, we have repeated the above analysis by replacing them with CRUTEM3 land temperature

datasets [*Jones,* 1996]. The results over the land regions are (figure not shown) qualitatively similar to those in Figure 10a, indicating that the NCEP/NCAR 2m temperature datasets over the study period can be reasonably used to understand the impacts of ENSO Modoki.

The unique impacts of El Niño during boreal summer on anomalies of surface air temperature after removal of the effects of the ENSO Modoki and IOD are shown in Figure 10b. In North America, significant positive correlations can be seen along the Pacific coast up to Alaska. We also find similar warm anomalies along the Pacific coast in South America. In contrast, significant negative correlations are seen over the northeastern parts of US and Canada. Significant negative correlations can also be seen over the maritime continent, eastern China and Japan in East Asia, Turkey and southern Mediterranean Europe, indicating cooler summers during El Niño. In South Asia, significant positive correlations can be seen. Significant positive correlations are also seen over Central and East Africa. We see that the impacts of the ENSO are opposite to those of ENSO Modoki over many regions such as tropical South America, equatorial Africa, and India. This again confirms that the ENSO Modoki is different from ENSO.

For completeness, we show the partial correlations between the IODMI and JJAS surface temperature in Figure 10c. Besides the familiar dipolar structure over the tropical Indian Ocean, correlations indicate that the positive IOD events cool the maritime region and north-central Australia significantly during austral winters. In contrast to the El Niño influence, southwest Australia significantly warms up during positive IOD events. Many regions in the northern hemisphere such as the Far East including Japan, the Mediterranean and Europe, US and central Canada experience warmer summer when a

positive IOD event occurs, in confirmation of earlier studies [*Saji and Yamagata*, 2003; *Guan and Yamagata*, 2003; *Yamagata et al.*, 2004].

2) Boreal winter season

The boreal winter (DJF) partial correlations of the EMI with the rainfall anomalies over the period 1979-2004, after removing the linear influence of NINO3 index, are presented in Figure 11a. Their robustness is verified in Figure A2-2 in the auxiliary information by the Monte Carlo method; The IOD events, in general, terminate by the end of November because of their strong seasonally phase-locked life cycle due to reversal of monsoonal winds over the equatorial Indian Ocean [*Saji et al.*, 1999; *Rao and Yamagata.*, 2004; *Rao et al.*, 2007], and hence the IOD influence is removed almost automatically. The equatorial eastern Pacific receives less than normal rainfall when El Niño Modoki is active. The positive partial correlations in the central equatorial region extend northeastward to Mexico. Some parts of the maritime countries, southern Thailand, the Philippines, southern India, Sri Lanka, and East Africa experience anomalous dry conditions. On the other hand, significantly wet conditions are seen over New Zealand, Pakistan, Kazakhstan, and parts of South Central Africa.

During El Niño events, as seen in Figure 11b, a wide area in the western Pacific region extending from the Philippines to Western Australia through the maritime continent experiences deficit rainfall. On the other hand, another wide region from the central to eastern equatorial Pacific receives above normal rainfall, which is very different from the impacts of El Niño Modoki. The southern part of the African continent, equatorial South America and northern New Zealand in the Southern

Hemisphere experience drier summer during El Niño, whereas regions of northern Argentina, southeast Brazil and Uruguay experience wetter summer. Significant wet conditions are also seen from northeast Africa to central India and further to Far East through southern China. We also note that North America receives above normal rainfall.

The most prominent impact of EMI events on surface temperature during boreal winter is, as expected, the warming over the central equatorial ocean and the cooling on both sides, i.e., over the eastern equatorial Pacific and over the maritime continent including the Philippines in Northern Hemisphere, and western and southern Australia in the Southern Hemisphere (Figure 12a). The west coast of Mexico may experience warmer winter. On the other hand, El Niño Modoki events appear to cause anomalously cold winters in eastern India and Eastern Europe. The subtropical east coast of South America also has cooler than normal austral summer.

El Niño impacts on boreal winter surface temperature seem to be more extensive and different from the El Niño Modoki impacts as seen in Figure 12b [see also *Yamagata and Masumoto*, 1992]. Except for the western tropical Pacific, the global tropical region in general is warmer during El Niño winters [cf. *Pan and Oort*, 1983]. This is particularly pronounced in the tropical Indian Ocean through changes of Walker circulation [cf. *Yamagata et al.*, 2004]. El Niño also brings warmer than normal boreal winters over the west coast of Mexico and US and along a zonal belt across the northern North America. Western inland Mexico is cooler during the same period. The region from the South China Sea to Japan is warmer than normal during El Niño winters. The eastern and southwestern Australian region is warmer than normal, whereas New Zealand

is colder than normal. Those impacts of El Niño are, in general, similar to earlier studies [e.g. *Diaz et al.*, 2001, *Saji and Yamagata*, 2003].

3) Possible teleconnection mechanisms

To understand possible mechanisms of the teleconnection pattern of the ENSO Modoki phenomenon, we have computed the JJAS partial correlations between the EMI and global SLPA after removing the influence of ENSO and IOD phenomena (Figure 13a). A large area in the central Pacific is covered by negative correlations that indicate anomalous depression of surface pressure during El Niño Modoki summers; the rest of tropical regions are covered by positive correlations indicating anomalous high pressure areas sandwiching the low pressure area in the center. The central negative correlations extend west towards northeast India via the Philippines and towards 120ºE through New Zealand in the southern hemisphere. The composite distribution of JJAS SLPA in summers of strong El Niño Modoki (figure not shown) is in agreement with Figure 13a. A similar composite distribution of the anomalous circulation at 850 hPa shows the central Pacific convergence of anomalous westerlies in the western equatorial Pacific and anomalous easterlies in the eastern equatorial Pacific (Figure 13b). The composite wind anomalies at 200 hPa over the tropical Pacific are opposite in sign in the same region (Figure 13c), indicating the presence of two anomalous Walker circulation cells in the troposphere. The joint ascending branch of these cells is located in the central equatorial Pacific. *This double cell pattern shows a marked difference from the single cell pattern in the typical El Niño case*. It is clearly seen when an El Niño Modoki event occurs during boreal winters, such as in DJF 2004/2005 (Figure 14). The anomalous circulation

in the tropical zonal-vertical plane is consistent with the surplus rainfall in the ascending region of the central tropical Pacific and the deficit rainfall in the descending regions. The precipitation anomaly distribution (Figures 9a and 9b) is basically consistent with the SLPA correlations (Figure 13a).

The impacts of the ENSO Modoki on the climate of the surrounding subtropical region may be attributed to the Rossby wavetrain generated by the diabatic heating in the central tropical Pacific [cf. *Wang et al.*, 2003; *Saji et al.*, 2005]. Another relevant hypothesis is given by *Trenberth et al*. [1998], who suggest that the Hadley circulation due to the tropical forcing induces changes in convergence/divergence patterns in subtropics that in turn act as Rossby wave source, subject to some constraints such as the location of heat source, interaction with the climatological stationary planetary waves.

As seen in Figures 13b and 13c, it is inferred that the atmospheric response to the El Niño Modoki is baroclinic in the tropics, whereas it has an equivalent barotropic structure in the subtropics. The basic mean state of mid-latitude atmospheric circulation plays an important role in transmitting the energy from the tropics to mid-latitudes [*Hoskins and Karoly*, 1981; *Trenberth et al.*, 1998; *Diaz et al.*, 2001, *Kidson et al.*, 2002]. The JJAS partial correlations of the EMI with geopotential anomalies at 500 hPa are shown in Figure15a. The response is uni-polar in the tropics and subtropics, and wavetrains can be seen in mid-latitudes of Northern Hemisphere. The response in the Southern Hemisphere appears to be a wavenumber 1 pattern. The DJF partial correlations between EMI and geopotential anomalies at 500 hPa (Figure 15b) indicate stronger response in the Northern Hemisphere. The stronger teleconnections in the winter hemisphere may be due to the phase-locking of the stronger subtropical and subpolar jet

streams that act as waveguides in carrying the energy from tropical heat sources [e.g. *Hoskins and Karoly*, 1981; *Webster*, 1982; *Diaz et al.*, 2001; *Wang et al.*, 2003; *Saji et al.*, 2004]. Also, the modulation of the jet stream intensity and location by the ENSO Modoki events, just as by the ENSO and IOD events [*Nakamura and Shimpo*, 2004, *Ashok et al.*, 2007a], may induce teleconnections in higher latitudes.

Another process through which the ENSO Modoki events may influence the East Asian region is possibly through a combination of two mechanisms, namely, the monsoon-desert mechanism [*Rodwell and Hoskins*, 1996] and the Silk Road pattern [*Enomoto et al.*, 2003][6]. The other, not alternative, way in which the ENSO Modoki may influence the East Asia, in particular, Japan, is through a mechanism analogous to the one proposed by *Nitta* [1987], which is popularly known as the Pacific-Japan (PJ) pattern[7]. This mechanism essentially involves a modulation of the tropical-subtropical Hadley circulation due to changes in the tropical SST. It is interesting to note that significantly drier and warmer conditions are seen over Japan during El Niño Modoki events; this impact is just opposite to that of El Niño events (Figures 9 and 10).

Though further details of the ENSO Modoki teleconnection mechanism have to be worked out, *the fact that impacts of the ENSO Modoki are quite different from those of*

6 The Indian monsoon is influenced by the tropical SSTA forcing during ENSO and IOD events. *Rodwell and Hoskins* [1996] suggested that the changes in Indian monsoon affect the Mediterranean /Sahel region through the long Rossby wave response, a process that is now known as monsoon-desert mechanism. While examining the evolution of the summer condition over Japan region, *Enomoto et al.* [2003] suggest that as the Asian jet acts as a waveguide to transmit the impact from Mediterranean region all the way up to East Asia. This process has been named as the Silk Road pattern. Several publications [*Guan and Yamagata*, 2003; *Saji and Yamagata*, 2003] indicate that the impacts IOD during boreal summer are carried to East Asian/Japan region by a combination of these mechanisms. We hypothesize that these mechanisms also may act during the El Niño Modoki events, and thereby transmit their impacts to higher latitudes in the northern hemisphere.

7 According to *Nitta* [1987], the SST in the tropical western Pacific (10ºN-20ºN, 150ºE-170ºE) are anomalously colder during a typical El Niño event. The convection is inactive over the Philippine Sea during such years. This induces an anomalous response further north, causing cool and wet (warm and dry) summers over Japan. During the typical La Niña years, in contrast, the SST anomalies are opposite over the aforementioned region, and consequently, impact over the East Asia is the opposite.

ENSO in many regions over the globe supports the uniqueness of the El Niño Modoki phenomenon.

4. Modulation of ENSO Modoki: possible links to background changes

The EOF2 pattern obtained from an EOF analysis of the tropical Pacific SSTA over the domain shown in Fig. 2a but for the period of 1958-78 (Figure 16) does not show any clear maximum variance in the central tropical Pacific; actually, it looks more like an ENSO (cf. Figures 2a and 2b). The ENSO Modoki is also not represented by the next two higher modes for this period. The maximum lead correlation of the PC1 with PC2 for this period, occurring at a lag of 10 months, is -0.6, indicating that about 36% of variability of EOF2 is related to ENSO, unlike for the period after 1978.

A similar EOF analysis of SSTA from an extended period from 1958 through 2004 indicates that the ENSO Modoki pattern appears as EOF3, explaining about 9% of the variance (figure not shown). We find that the ENSO Modoki events that have been identified in the present study based on EMI are also well represented by the PC3 from the extended period EOF analyses. The events prior to 1979 were relatively weak and short-lived, and hence the relatively low variance explained the EOF3; A hint of this is also obtained from similar EOF analyses by Meyers et al. (1999) based on the datasets from 1868-1993. This indicates that increase in the ENSO Modoki events after 1979 has enhanced their role in tropical Pacific variability.

These analyses confirm that ENSO Modoki is relatively dominant in the tropics after 1978 as compared to the earlier period, and that a large portion of ENSO Modoki variability is not associated with the ENSO phenomenon since 1979. The occurrence and

life period of the ENSO Modoki events have increased since the early 1980s, and hence the ENSO Modoki events appear as one of the top two dominant modes of the tropical Pacific SST variability, each of which seems to be associated with its own distinct nature of tropical coupled dynamics. It will be interesting to discuss possible reasons for the recent increase in variance explained by such a higher coupled mode. Figure 17a shows the long-term change in mean SST, obtained by subtracting the mean SST for the period 1958-1978 from that for the period 1979-2004. This difference distribution, which can be interpreted as either a long-term trend or an interdecadal change, shows general warming over most of the globe between 60ºS and 60ºN except for the northern North Pacific where there is significant cooling as described in *IPCC* [2001], *Deser et al*. [2004], and *Hartmann and Wendler* [2005]. Interestingly, maximum SST warming regions in the tropical Pacific are located just off the equator in the eastern Pacific. We have also verified that the annual SST climatology difference is in agreement with the heat content changes at 300 meters depth (figure not shown). This sort of SST trend in the equatorial Pacific is associated with the low-level wind trend (Figure 17a). We see that most of the area of the tropical Pacific is dominated by enhanced westerly anomalies, indicating that equatorial easterly winds have weakened as discussed by *Inoue and O'Brien* [1987], *Kitamura* [1990] and *Yamagata and Masumoto* [1992; see their Figure 17b]; we further confirm the weakening of the low level easterly winds by a similar analysis (figure not shown) based on ERA-40 datasets [*Simons and Gibson*, 2000]. The weakened easterlies over the equatorial central Pacific and enhanced easterlies in the eastern Pacific weaken the zonal gradient of SST as well as the zonal tilt of the thermocline. The relative flattening of the thermocline in the recent period can be seen by calculating the difference

of isotherms in two different periods (Figure 17c). This finding is in agreement with the ocean temperature trend in the equatorial Pacific for the period 1945-93, as shown in an earlier study [e.g. Figure 2a of *Liu and Huang*, 2000]. The change related to weakening of low-level easterlies in the central equatorial Pacific reflects the present climate state that favors the formation of more El Niños as compared to La Niñas [e.g. *Namias et al.*, 1988; *Nitta and Yamada*, 1989; *Fedorov and Philander*, 2000; *Philander*, 2004. This also means that the present day climate is less conducive to turnabout of ENSO events as compared to the period of 1960-1978. Another way to describe this trend is to introduce a concept of El Niño-like decadal phenomenon [*Luo and Yamagata*, 2001; *Annamalai et al.*, 2005; *Lohman and Latif*, 2005]. However, we here suggest that such a trend may be attributed to the recent frequent occurrence of the ENSO Modoki event.

The EOF3 structure shown in Figure 2c and its associated principal component PC3 shown in Figure 3 provide potential clues to interpret the recent decadal changes in ENSO Modoki occurrence in terms of background changes. It is interesting that the PC3 exhibits a long-term increasing trend since 1979. It is also seen that after 2001, the PC3 was in such a phase that strengthens the SSTA gradient between the central tropical Pacific and eastern tropical Pacific, there by increasing the El Niño Modoki condition. The magnitude of the correlation between PC2 and PC3 for the period 1998-2004 increased to 0.71, showing that the modes were in tandem during this period. This has some implications for the strength of ENSO Modoki. For example, the major contribution to the tropical Pacific summer SSTA in 2004 is from EOF2 (figure not shown). This structure is enhanced in the central and eastern tropical Pacific by contribution from EOF3 (figure not shown). The long term phase of the PC3 has changed around 1987-88,

and this appears to be associated with a further increase in ENSO Modoki frequency thereafter.

5. Summary and discussion

We have identified a new tropical Pacific ocean-atmosphere coupled phenomenon that is named as El Niño Modoki (Pseudo-El Niño) in this article. A typical example of a positive phase of this phenomenon is found in 2004, with warming in the central tropical Pacific, flanked by anomalously colder than normal SSTA in the western and eastern Pacific. The event is different from the conventional ENSO event. An EOF analysis performed on the monthly SSTA from 1979 to 2004 shows that the El Niño Modoki is similar to the EOF2 pattern that explains about 12% of the tropical Pacific SST variability.

Using a composite analysis method, we have demonstrated the physical existence of El Niño Modoki and its unique impact on the world climate. The composite and correlation analyses of SSH, SST, ocean subsurface temperature, and zonal wind anomalies indicate that the El Niño Modoki is an ocean-atmosphere coupled phenomenon which is distinct from El Niño. The central SST warming and associated zonal wind convergence on either side of the SSTA sustain the event for almost a year. Interestingly, the coupled mode appears almost as a standing mode in the central Pacific, and does not evolve into a full-fledged El Nino event. The partial correlation analysis identifies many regions over the world where the temperature and rainfall are significantly influenced by the ENSO Modoki phenomenon during boreal summer as well as boreal winter. In the tropics, this extensive impact is due to anomalous twin Walker circulation cells with their

common updraft branch centered over the central tropical Pacific pole of the SSTA tripole of ENSO Modoki. The impacts are transmitted to higher latitudes as in the cases of ENSO and IOD. The impacts propagate into the winter hemisphere more efficiently because of relatively stronger seasonal subtropical and subpolar jet streams, which is in agreement with many past studies related to ENSO teleconnection.

Because of its double cell structure in the atmosphere in accord to the tripole structure in SSTA, the ENSO Modoki may be classified as a higher coupled mode compared to the gravest ENSO mode. The present study also shows that most of the ENSO Modoki events during the study period are not a part of ENSO evolution. The background state during the present warm climate appears to be relatively less conducive to the turnabout of ENSO events in comparison with the period 1958-78; it appears more conducive to rather persistent occurrence of the ENSO Modoki. A recent study by *Monahan and Dai* [2004] suggests that the temporal and spatial nonlinear relationship of the first two modes of the tropical Pacific SST variability leads to the nonlinear structures of El Niño and La Niña. This nonlinear relationship may also be subject to the changes in the background conditions. Also, there is certainly asymmetry in the strengths of El Niño and La Niña in real world. This asymmetry (Rodgers et al., 2004; An and Jinn, 2004) *per se*, however, can not result in ENSO Modoki owing to the reason that both El Niño and La Niña do not occur simultaneously. However, a very strong El Niño can leave some residual signal. This residual, in turn, can interact with a following La Niña and manifest as a Modoki; this sort of scenario can be interpreted as a change in background conditions. Yet, it should also be noted that Modoki events such as 2004 have no preceding strong signals of ENSO, as already discussed.

We suggest that ENSO and ENSO Modoki comprise two major orthogonal modes of the ocean-atmosphere coupled system in the tropical Pacific. Based on the background state, the Pacific coupled system may prefer one of these dominant coupled modes. Rather than referring to ENSO Modoki as a part of ENSO by changing the definition of ENSO, we have proposed another way to view the recent climate conditions in the tropical Pacific from a new angle.

There are several aspects that need further investigation about the ENSO Modoki introduced in the present paper. Its teleconnection needs to be studied in more detail using observational data and coupled models. Also, most of the processes discussed here are subject to severe limitation of a linearized view. Nevertheless, the ENSO Modoki, just like other climate element modes such as ENSO and IOD, appears to be important in deepening our understanding of global climate variability. The reason why the ENSO Modoki occurs more frequently and persistently in recent decades also needs thorough investigation from a viewpoint of the global warming trend. Another interesting direction of research is to examine the potential role of intraseasonal wind bursts (McPhaden 2004) which may trigger these climate modes in a different way under different background conditions by influencing the propagation of the coupled downwelling Kelvin waves [*Ashok et al.*, 2007b]. Considering the increasing importance of the ENSO Modoki event in the recent tropical Pacific variability, attempts to predict the phenomenon should also be started; this will lead to better seasonal prediction, and certainly benefit our society.

Acknowledgements

The senior author (TY) is encouraged by Mr. M. Yamamoto, a reporter of Kyodo News, to develop the present concept of ENSO Modoki in the early summer of 2004. The authors acknowledge Dr. Gary Meyers for the discussion on Australian droughts, and Dr. J-J. Luo for discussion on the decadal changes in the tropical Pacific. Drs. R. Lukas, J. McCreary, Z. Liu, H. Annamalai and T. Tozuka are thanked for their helpful suggestions and comments on an earlier version. Constructive comments from three anonymous referees and Dr. James Richman helped to improve this manuscript. Useful comments from an anonymous reviewer of an earlier version are also acknowledged. The Pacific decadal oscillation index has been downloaded from http://www.atmos.washington.edu/~mantua/abst.PDO.html. Figures in this paper have been prepared using the GrADs (COLA), and FERRET softwares.

APPENDIX I

Figure A1-1: The phase information of complex EOF1 (top left) and complex EOF2 (top right) of SSTA. Similar information for SSHA is provided in the middle panels. The bottom panels provide the respective principal components, with thick (dashed) lines representing the SSTA (SSHA).

Figure A1-2: The amplitude of complex EOF1 (top left) and complex EOF2 (top right) of SSTA. Similar information for SSHA is provided in the middle panels. The bottom panels provide the respective principal components, with thick lines representing the SSTA and dashed lines for SSHA.

APPENDIX II

The partial correlation coefficient $r_{12.3}$ between two variables A_1, A_2, after removing the influence of the variable A_3, is given by

$$r_{12,3} = \frac{r_{12} - r_{13}\, r_{23}}{\sqrt{(1 - r_{13}^2)(1 - r_{23}^2)}} \qquad (1)$$

In equation (1) the term r_{ij} represents the linear correlation coefficient between A_i and A_j. The partial coefficient $r_{12.34}$ between two variables A_1, A_2, after removing the influence of the variables A_3 and A_4, is obtained by

$$r_{12,34} = \frac{r_{12,4} - r_{13,4}\, r_{23,4}}{\sqrt{(1 - r_{13,4}^2)(1 - r_{23,4}^2)}} = \frac{r_{12,3} - r_{14,3}\, r_{24,3}}{\sqrt{(1 - r_{14,3}^2)(1 - r_{24,3}^2)}} \qquad (2)$$

(equivalent to Equation 7.2 of *Pedhazur* ,1997; also see Ashok et al., 2007a).

The number of degrees of freedom for seasonal partial correlations was fixed at N-3 for the first order, and N-4 for the second order, N being the number of values in the time series. Further details are available from *Wilks,* 1995*; Pedhazur,* 1997; *Spiegel,* 1997, *Ashok et al.* 2007a etc. We also reconfirm the significance of the seasonal correlations over many regions of the globe by carrying out 1000 Montecarlo simulations [broadly after *Saji and Yamagata*, 2003]. To do this, we first generate 1000 sets of time series of random numbers which have the variance of the independent time series, such as EMI; the autocorrelation present in the original time series at Lag 1 is also preserved [for technical details, see *Broomhead and King* 1976; *Burg* 1978; *Marsalia* 1990; *Vautard et al.,* 1992]. These randomized time series are then used to compute the partial correlations with rainfall/temperature fields. After sorting the 1000 partial correlations, we designate the 900th highest value as the significant value at a 90% confidence level.

We have also taken the autocorrelations of all the *monthly* time series into consideration when fixing the degrees of freedom for them [after *Davis et al*, 1976].

REFERENCES

Aceituno, P. (1988), On the functioning of the Southern Oscillation in the South American sector. Part I: Surface climate. *Mon. Wea. Rev.*, *116,* 505–525.

Adler, R.F., G.J. Huffman, A. Chang, R. Ferraro, P. Xie, J. Janowiak, B. Rudolf, U. Schneider, S. Curtis, D. Bolvin, A. Gruber, J. Susskind, and P. Arkin (2003), The Version 2 Global Precipitation Climatology Project (GPCP) Monthly Precipitation analysis (1979 - Present) *J. Hydrometeor., 4,* 1147-1167.

Allan, R. J., C. J. C. Reason, J. A. Lindesay, T. J. Ansell, (2003), 'Protracted' ENSO episodes and their impacts in the Indian Ocean region. *Deep.Sea.Res. II, 50,* 2331-2347.

An, S.-I., and F-F Jin (2004): Non-linearity and asymmetry of ENSO. *J. Climate*, *17,* 2399-2412.

Annamalai, H., J. Potemra, R. Murtugudde, and J.P. McCreary (2005), Effect of preconditioning on the extreme climate events in the tropical Indian Ocean. *J. Climate*, *18,* 3450–3469.

Ashok, K., Z. Guan and T. Yamagata (2001), Impact of the Indian Ocean Dipole on the relationship between the Indian Monsoon rainfall and ENSO, *Geophys. Res. Lett., 28*, 4499-4502.

Ashok, K., Z. Guan and T. Yamagata (2003), Influence of the Indian Ocean dipole on the Australian winter rainfall. *Geophys. Res. Lett., 30*(15), 1821, doi:10.1029/2003GL017926.

Ashok, K., Z. Guan, N. H. Saji, and T. Yamagata (2004), Individual and combined influences of the ENSO and Indian Ocean Dipole on the Indian summer monsoon. *J. Climate, 17,* 3141-3155.

Ashok, K., H. Nakamura, and T. Yamagata (2007a), Impacts of ENSO and IOD events on the Southern Hemisphere storm track activity during austral winter (in press, *J. Climate*).

Ashok, K., S. K. Behera, S. A. Rao, H. Weng, and T. Yamagata (2007b), An unusual coupled mode in the tropical Pacific during 2004 (submitted to *Geophys. Res. Lett.*).

Behera, S. K., and T. Yamagata (2001), Subtropical SST dipole events in the southern Indian Ocean, Geophys. Res. Lett., *28,* 327-330, 10.1029/2000GL011451.

Behera, S. K., J.-J. Luo, S. Masson, P. Delecluse, S. Gualdi, A. Navarra, and T. Yamagata (2005), Paramount Impact of the Indian Ocean Dipole on the East African Short Rains: A CGCM Study, *J. Climate, 18*, 4514-4530.

Bjerknes, J. (1969), Atmospheric teleconnections from the euqatorial Pacific, *Mon. Wea. Rev., 97*, 163-172.

Broomhead, D.S., and King, G. (1986), Extracting qualitative dynamics from experimental data, *Physica D, 20,* 217-236.

Burg, J. P. (1978), A new analysis technique for time series data. In Modern Spectrum Analysis, D. G. Childers (ed.), pp. 42-48, IEEE Press, N.Y.

Carton, J.A., and B.S. Giese (2007), SODA: A Reanalysis of Ocean Climate, *J. Geophys. Res.* (submitted).

Carton, J.A., and B.S. Giese, and S. A. Grodsky (2005), Sea level warming of the oceans in the simple Ocean data assimilation (SODA) ocean reanalysis, *J. Geophys. Res., 110,* C090006, doi: 10.1029/2004JC002817.

Davis, R. E. (1976), Predictability of Sea surface temperature and sea level pressure anomalies over the North Pacific ocean. *J. Phys. Oceanogr., 6,* 249-266.

Diaz, H. F., M. P. Hoerling, and J. K. Eischeid (2001), ENSO variability, teleconnections and climate change. *Int. J. Climatol., 21,* 1845-1862.

Deser, C., A.S. Phillips, and J.W. Hurrell (2004), Pacific interdecadal climate variability: Linkages between the tropics and the north Pacific during boreal winter since 1900. *J. Climate*, *17*, 3109–3124.

Donguy J-R., and A. Dessier (1983), El Niño-like events observed in the tropical Pacific, *Mon. Wea. Rev., 111*, 2136-2139.

Enomoto, T., B. Hoskins, and Y. Masuda (2003), The formation of Bonin high in August, *Q. J. R. Meteorol. Soc., 587,* 157-178.

Fedorov, A. V., and S. G. Philander (2000), Is El Niño changing? Science, *288,* 1997-2002.

Hartmann, B., and G. Wendler (2005), The significance of the 1976 Pacific climate shift in the climatology of Alaska. *J. Climate*, *18*, 4824–4839.

Hoskins, B. J., and D. Karoly (1981), The steady liner response of a spherical atmosphere to thermal and orographic forcing. *J. Atmos. Sci., 38,* 1179-1196.

Guan, Z., and T. Yamagata (2003), The unusual summer of 1994 in East Asia: IOD teleconnections. *Geophys. Res. Lett., 30,* 1544, doi:10.1029/2002GL016831.

Inoue, M., and I. J. O'Brien (1987), Trends in sea level in the western and central equatorial Pacific during 1974-1975 to 1981. *J. Geophys. Res.*, *92,* 5045-5051.

IPCC (2001), Climate Change 2001: Synthesis Report. A Contribution of Working Groups I, II, and III to the Third Assessment Report of theIntegovernmental Panel on Climate Change [Watson, R.T. and the Core Writing Team (eds.)]. Cambridge University Press, Cambridge,United Kingdom, and New York, NY, USA, 398 pp.

Jones, P.D., New, M., Parker, D.E., Martin, S. and Rigor, I.G., (1999), Surface air temperature and its variations over the last 150 years. *Reviews of Geophysics 37*, 173-199.

Kalnay, E., and coauthors (1996), The NCEP/NCAR 40-year reanalysis project. *Bull. Amer. Meteor. Soc.,* **77**, 437-471.

Kidson, J. W., M. J. Revell, B. Bhaskaran, A. B. Mullan, and J. A. Renwick (2002), Convection patterns in the tropical Pacific and their influence on the atmospheric circulation at high latitudes. *J. Climate, 15,* 137-159.

Kistler, R., and coauthors (2001), The NCEP-NCAR 50-year reanalysis: monthly means CD-ROM and documentation. *Bull. Amer. Meteor. Soc., 82,* 247-268.

Kitamura, Y. (1990), Simulation of the annual and interannual variation of the tropical Pacific Ocean. *J. Mar. Systems*, *1,* 169-181.

Larkin N. K., and D. E. Harrison (2005a), On the definition of El Niño and associated seasonal average U.S. weather anomalies. *Geophys. Res. Lett., 32,* L13705, doi:10.1029/2005GL022738.

Larkin N. K., and D. E. Harrison (2005b), Global seasonal temperature and precipitation anomalies during El Niño autumn and winter. *Geophys. Res. Lett., 32,* L16705, doi:10.1029/2005GL022860.

Levitus, S., J. Antonov, and T. Boyer (2005), Warming of the world ocean, 1955-2003. *Geophys. Res. Lett., 32,* L02604, doi:10.1029/2004GL021592.

Liu, Z., and B. Huang (2000), Cause of tropical Pacific warming trend. *Geophys. Res. Lett., 27,* 1935-1938.

Lohmann, K., and M. Latif (2005), Tropical Pacific decadal variability and the subtropical cells, *J. Climate, 18,* 5163-5178.

Luo, J., and T. Yamagata (2001), Long-term El Niño-Southern Oscillation (ENSO)-like variation with special emphasis on the South Pacific. *J. Geophys. Res.*, *106*(C10), 22,211–22,228.

Mantua, N.J. and S.R. Hare, Y. Zhang, J.M. Wallace, and R.C. Francis (1997), A Pacific interdecadal climate oscillation with impacts on salmon production. *Bulletin of the American Meteorological Society, 78,* 1069-1079.

Marsaglia, G., Zaman, A., and Tsang, W.W. (1990), Toward a universal random number generator, *Stats & Prob Letters*, *8*, 35-39.

McPhaden, M. J. (2004), Evolution of the 2002/03 El Niño *Bulletin of the American Meteorological Society, 85*, 677-695.

Meyers, S. D., J. J. O' Brien, and E. Thelin (1999), Reconstruction of monthly SST in the tropical Pacific Ocean during 1868-1993 using adaptive climate basis functions. *Mon. Wea. Rev., 127,* 1599-1612.

Meyers, G., P. Mcintosh, L. Pigot, and M. Pook (2007), The years of El Niño, La Niña and interactions with the tropical Indian Ocean, *J. Climate* (in press).

Monahan, A. H., and A. Dai (2004), The spatial and temporal structure of ENSO non-linarity, *J. Climate*, *17,* 3026–3036.

Navarra et al.. A., M. N. Ward, and K. Miyakoda (1999), Tropical-wide teleconnections and oscillation. I: Teleconnection indices and type I/II states, *Q. J. R. Meteorol. Soc., 125,* 2909-2935.

Nakamura, H., and A. Shimpo (2004), Seasonal variations in the Southern Hemisphere storm tracks and jet streams as revealed in a reanalysis dataset. *J. Climate, 17,* 1828-1844.

Namias, J., X. Yuan, and D. R. Cayan (1988), Persistence of North Pacific sea surface temperature andatmospheric flow patterns. *J. Climate*, *1,* 682-703.

Nitta, T. (1987), Convective activities in the tropical Pacific and their impacts on the northern hemisphere summer circulation. *J. Meteor. Soc. Japan, 65,* 373-390.

Nitta, T., and S. Yamada (1989), Recent warming of tropical sea surface temperature and its relationship to the northern hemisphere circulation. *J. Meteor. Soc. Japan, 67,* 375-383.

North, G. R., T. L. bell, and R. F. Chalan (1982), Sampling erros in the estimation of empirical orthogonal functions. *Mon. Wea. Rev., 110,* 699-706.

Pan, Y-H., and A. H. Oort (1983), Global climate variations connected with sea surface temperature anomalies in the eastern equatorial Pacific Ocean for the 1958-73 period. *Monthly Weather Review, 111,* 1244-1258.

Pedhazur, E. J. (1997), Multiple regression in behavioural research: explanation and prediction. Third edition U.S. A. Holt, Rinchart and Winston, Inc.

Philander, S. G. H. (1990), *El Niño, La Niña and the Southern Oscillation,* Academic Press, San Deiego, Calif., 293 pp.

Philander, S. G. H. (2004), *Our Affair with El Niño: How We Transformed an Enchanting Peruvian Current into a Global Climate Hazzard*. Princeton, NJ: Princeton University Press, 296 pp.

Rao, S.A., and T. Yamagata (2004), Abrupt termination of Indian Ocean Dipole events in response to intraseasonal disturbances *Geophys. Res. Lett., 31,* L19306, doi:10.1029/2004GL020842.

Rao, S.A., and S. K. Behera (2005), Subsurface influence on SST in the tropical Indian Ocean: structure and interannual variability *Dyn. Atmos. Ocean.* , *39,* 103-135.

Rao, S.A.,, S. Masson, J-J. Luo, S. K. Behera, and T. Yamagata (2007), Termination of Indian Ocean Dipole events in a general circulation model (in press, *J. Climate).*

Rasmusson, E. M., and T. H. Carpenter (1982), Variation in tropical sea surface temperature and surface wind fields associated with Southern Oscillation/El Niño, *Mon. Wea. Rev., 110,* 354-384.

Rayner, N. A., D. E. Parker, E. B. Horton, C. K. Folland, L. V. Alexander, D. P. Rowell, E. C. Kent, and A. Kaplan (2003), Global analyses of sea surface temperature, sea ice, and night marine air temperature since the late nineteenth century , *J. Geophys. Res.*, *108,* No. D14, 4407 doi:10.1029/2002JD002670.

Reynolds, R. W., N. A. Rayner, T. M. Smith, D. C. Stokes and W. Wang (2002), An Improved In Situ and Satellite SST Analysis for Climate**.** *J. Climate*, *15,* 1609–1625.

Richman, M. B. (1986), Rotation of principal components *J. Climatol., 6,* 293-335.

Rodgers, K. B., P. Friederichs, M. Latif, (2004), Tropical Pacific decadal variability and its relationship to decadal modulations of ENSO, *J. Climate*, *17*, 3761-3774

Rodwell, M. J. and B. J. Hoskins (1996), Monsoons and the dynamics of deserts, , *Q. J. R. Meteorol. Soc., 122,* 1385-1404.

Ropelewski, C.F., and M.S. Halpert, North American precipitation and temperature patterns associated with the El Nino/Southern Oscillation (ENSO) (1987), *Mon. Wea. Rev*., *114,* 2352-2362.

Saji, N. H., B. N. Goswami, P. N. Vinayachandran and T. Yamagata (1999), A dipole mode in the tropical Indian Ocean. *Nature*, *401,* 360-363.

Saji, N. H., and T. Yamagata (2003), Possible impacts of Indian Ocean Dipole events on global climate, *Climate Res., 25,* 151-169.

Saji, N. H., , T. Ambrizzi, and S. E. T. Ferraz (2005), Indian Ocean Dipole mode events and austral surface air temperatures. *Dyn. Atmos. Ocean*., *39,* 87-102.

Simmons, A. J., and J. K. Gibson (2000), The ERA-to project plan, ERA-40 project report series No. 1, ECMWF, Reading RG2 9AX, UK, 63pp.

Spiegel, M. R. (1997), Statistics, *Schaum's outline of theory and problems of statistics,* 520pp.

Stephens, C., S. Levitus, J. Antonov, and T. Boyer (2001), The Pacific regime shift, *Geophys. Res. Lett.*, *28*, 3721–3724.

Tozuka, T., and T. Yamagata (2003), Annual ENSO. *Journal of Physical Oceanography, 33,* 1564–1578.

Trenberth, K. E., G. W. Branstator, D. Karoly, A. Kumar, N.-C. Lau, C. Ropelewski (1998), Progress during TOGA in understanding and modeling global teleconnections associated with tropical sea surface temperatures, *J. Geophys. Res., 103*(C7), 14291-14324, 10.1029/97JC01444.

Trenberth, K. E., D. P. Stepaniak, J. W. Hurrell and M. Fiorino (2001), Indices of El Nino evolution, *J. Climate,* 14, 1697-1701.

Trenberth, K. E., D. P. Stepaniak, J. W. Hurrell and M. Fiorino (2001), Quality of Reanalyses in the Tropics. *J. Climate, 14,* 1499–1510.

Trenberth, K. E., D.P. Stepaniak, and J.M. Caron (2002a), Interannual variations in the atmospheric heat budget. *J. Geophys. Res*., *107,* 4066, 10.1029/2000JD000297.

Trenberth, K. E., J. M. Caron, D. P. Stepaniak and S. Worley (2002b), The evolution of ENSO and global atmospheric temperatures. *J. Geophys. Res*., *107,* 4065, doi:10.1029/2000JD000298.

Vautard, R., P. Yiou, and M. Ghil (1992), Singular Spectrum Analysis: A toolkit for short, noisy, chaotic time series, *Physica D, 58*, 95-126.

Walker, G. T. (1923), correlations in seasonal variations of weather, VIII. A preliminary study of world weather I, *Mem. India. Meteorol. Dept., 23,* 75-131.

Walker, G. T. (1924), correlations in seasonal variations of weather, IX. *Mem. India. Meteorol. Dept., 24,* 275-332.

Wang, B., R. Wu, and T. Li (2003), Atmosphere-warm ocean interaction and its impact on Asian-Australian monsoon variability, *J. Climate, 16,* 1195-1211.

Weare, B.C., A.R. Navato, R. E. Newell (1976), Empirical orthogonal analysis of Pacific sea surface temperatures, *Journal of Physical Oceanography*, *6*(5), 671-678.

Webster, P, J. (1982), Seasonality in the local and remote atmospheric response to sea surface temperatures. *J. Atmos. Sci., 39,* 41-52.

Weng, H., K. Ashok, S. K. Behera, S. A. Rao, and T. Yamagata (2007), Impacts of recent El Niño Modoki dry/wet conditions in the Pacific rim during Boreal Summer, *Climate Dynamics*, 10.1007/s00382-007-0234-0.

Wilks, D. S. (1995), Statistical methods in the atmospheric Sciences: an introduction,Academic press, A dividion of Harcourt Brace & Company, 525 B street, Suite 1900, San Diego, CA, U.S. A., 467 pp.

World Meteorological Organization (2005), El Niño update 20 April 2005 (http://www.wmo.ch/index-en.html).

Xie, P., and P. A. Arkin (1996), Analyses of global monthly precipitation using rain gauge observations, satellite estimates and numerical model predictions. *J. Climate, 9*, 840-858.

Yamagata, T., and Y. Masumoto (1992), Interdecadal natural climate variability in the western Pacific and its implication in global warming. *J. Meteor. Soc. Jpn.*, *70,* 167-175.

Yamagata, T., S. K. Behera, J-J. Luo, S. Masson, M. R. Jury and S. A. Rao (2004), The coupled ocean-atmosphere variability in the tropical Indian Ocean. Earth's climate: The ocean-atmosphere interaction. *Geophysical Monograph, 147***,** AGU, pp 189-211.

Yin, X., A. Gruber, and P. Arkin (2004), Comparison of the GPCP and CMAP Merged Gauge–Satellite Monthly Precipitation Products for the Period 1979–2001. *Journal of Hydrometeorology*, *5,* 1207–1222.

Zhang, Y., J.M. Wallace, D.S. Battisti (1997), ENSO-like interdecadal variability: 1900-93. *J. Climate*, *10,* 1004-1020.

FIGURE CAPTIONS

Figure 1 Anomalous conditions during JJAS 2004 (a) for rainfall in cm/month (b) SST in ºC. The datasets of Version 2 Global Precipitation Climatology Project Monthly Precipitation Analysis [*Adler et al.*, 2003], and the Hadley Centre Global Sea Ice and Sea Surface Temperature (HadISST) Analyses [*Rayner et al.,* 2003] for the period 1979-2004 were used to obtain Figures 1a and 1b respectively.

Figure 2 Top four EOF modes of tropical Pacific SSTA (1979-2004) multiplied by respective standard deviations of the principal components; units in ºC.

Figure 3 Normalized time series of PC1 (solid line), PC2 (bar), and PC3 (dashed line).

Figure 4 (a) Time series of normalized ENSO Modoki index (EMI; in bar) and that of the PC2 (thin line). The standard deviation of the EMI is 0.52ºC. (b) time series of Nino3.4 (solid thick line) index, and TNI (dashed thin line) as defined by Trenberth and Stepaniak (2001). Also shown is the time series of the *inverted* EMI (shaded). The sign of the EMI has been deliberately reversed in this figure to facilitate easy comparison of its evolution with the TNI.

Figure 5 Composite SSTA in ºC during strong positive El Niño Modoki events averaged over (a) seven boreal summers, namely JJAS seasons of 1986,1990, 1991, 1992, 1994, 2002 and 2004 and (b) 8 boreal winters, namely DJF seasons of 1979-80, 1986-87,1990-91, 1991-92, 1992-93, 1994-95, 2002-2003 and 2004-05. Significant values above 95% confidence level from a two tailed Student's t-test are shaded.

Figure 6 Lag/lead correlations of monthly EMI with sea surface height anomalies (shading) and ocean temperature anomalies at 10 meter depth (contours). Positive

(negative) correlation coefficients correspond to high (low) of sea level anomalies. Regressed winds with EMI are shown only if the correlation coefficient between EMI and respective wind components exceeds 0.24. Significant correlations at a 80%(90%) confidence level are 0.24 (0.3) from a 2-tailed Student's t-test after taking into account the autocorrelations of EMI). The positive (negative) numbers to the left of each panel indicate the months by which the EMI leads (lags) the anomaly distribution fields. The thin line extending from (b) to (e) side indicates the propagation of off-equatorial Rossby waves.

Figure 7 Lag/lead correlations of monthly EMI with sea level pressure anomalies. The positive (negative) numbers to the left of each panel indicate the months by which the EMI leads (lags) the anomaly distribution fields.

Figure 8 Lag/lead correlations of EMI with ocean subsurface temperature anomalies at different depths in meters averaged over 2ºS-4ºS. The positive (negative) numbers to the left of each panel indicate the months by which the EMI leads (lags) the anomaly distribution fields.

Figure 9 (a) Composite JJAS GPCP rainfall anomalies (cm/month) during strong positive El Niño Modoki events averaged over seven boreal summers, namely JJAS seasons of 1986, 1990, 1991, 1992, 1994, 2002 and 2004. (b) JJAS (1979-2004) partial correlations of GPCP rainfall anomalies with EMI. Only significant values at 90% confidence level from a 2-tailed Student's t-test are shown; positive (negative) correlations are in shading (contours). The contours shown are -0.34, -0.4, -0.5, -0.6 and -0.7. See text for details. (c) Same as Figure 9b but with NINO3 index. (d) Same as Figure 9b but with IODMI.

Figure 10 JJAS (1979-2004) partial correlations between temperature (2m height) anomalies and (a) EMI (b) NINO3 index (c) IODMI. Only significant values at 90% confidence level from a 2-tailed Student's t-test are shown; positive (negative) correlations are in shading (contours). The contours shown are -0.34, -0.4, -0.5, -0.6 and -0.7.

Figure 11 DJF (1979-2004) partial correlations between GPCP rainfall anomalies and EMI, significant at 90% confidence level from a two tailed Student's t-test; positive (negative) correlations are in shading (contours). The contours shown are -0.34, -0.4, -0.5, -0.6 and -0.7. (b) DJF (1979-2004) partial correlations between GPCP rainfall anomalies and NINO3 index.

Figure 12 (a) Same as Figure 10b but for DJF season (b) Same as Figure 10c but for DJF season.

Figure 13 (a) JJAS (1979-2004) partial correlations between SLPA and EMI. Shaded values are significant at 90% confidence level from a two tailed Student's t-test; negative (positive) correlations are in shading (contours). The contours shown are 0.34, 0.4, 0.5, 0.6 and 0.7. (b) Composite JJAS 850 hPa anomalous winds obtained from seven strong El Niño Modoki events. Shaded reasons indicate zonal winds significant at 90% confidence level from a two tailed Student's t-test. (c) Same as Figure 13b but at 200 hPa level.

Figure14 2004/05 DJF anomalous Walker circulation streamlines averaged from 10ºS to 10ºN.

Figure15 JJAS (1979-2004) partial correlations between 200 hPa geopotential anomalies and EMI. Significant values at 90% confidence level from a 2-tailed Student's t-test are

shown; negative (positive) correlations are in shading (contours). The contours shown are 0.34, 0.4, 0.5, 0.6 and 0.7.

Figure 16 EOF2 mode of tropical Pacific SSTA (1958-1978) multiplied by its standard deviations of the principal component; units in ºC. This mode explains about 10% of the tropical Pacific SSTA variance.

Figure 17 (a) Long term changes in mean SST (ºC) and winds at 1000 hPa (m/s), obtained by subtracting the mean SST of the period 1958-1978 from that over the period 1979-2004. (b) Long term changes in annual mean zonal winds at 1000 hPa (m/s), obtained similar as in Figure 17a. (c) Differences of ocean temperature in two periods of 1958-78 and 1978-2004 along with the depth-longitude section of climatological ocean temperature (black contours).

Table 1: Definitions of different regions/SSTA-based indices used in this study

Index Name	Definition
NINO3.4	The region is bounded by (5ºN-5ºS, 170ºW-120ºW). The area-averaged sea surface temperature anomaly (SSTA) over this region is known as NINO3.4 index
NINO3	The region is bounded by (5ºN-5ºS, 150ºW-90ºW). The area-averaged sea surface temperature anomaly over this region is known as NINO3 index, which is a well-known ENSO index.
NINO1+2	The region is bounded by (equator-10ºS, 90ºW-80ºW). The area-averaged sea surface temperature anomaly over this region is known as NINO1+2 index.
NINO4	The region is bounded by (5ºN-5ºS, 160ºE-150ºW). The area-averaged sea surface temperature anomaly over this region is known as NINO4 index.
Trans-Nino index	Defined as difference between normalized SSTA between NINO4 and NINO1+2 (Trenberth and Stepaniak, 2001).
Indian Ocean Dipole Mode Index	The Indian Ocean Dipole Mode Index (IODMI) is defined as the SSTA difference between the western (50ºE-70ºE, 10ºS-10ºN) and southeastern (90ºE-110ºE, 10ºS-equator) regions of the tropical Indian Ocean (Saji et al., 1999).
Subtropical Dipole Mode Index	The Indian Ocean Subtropical Dipole Mode Index (SDI) is defined as the SSTA difference between the western subtropical (55ºE-65ºE, 37ºS-27ºS) and southeastern (90ºE-100ºE, 28ºS-18ºS) regions of the subtropical Indian Ocean (Behera and Yamagata, 2001).
El Niño Modoki index	See the details in the text that follows equation 1 of this paper

Table 2: Correlation values of the El Niño Modoki index (EMI) with other indices in the tropical and subtropical Indo-Pacific region

	NINO3	NINO4	NINO3.4	IODMI	SDI
EMI	0.13	0.73	0.43	0.06	0.02

(a)

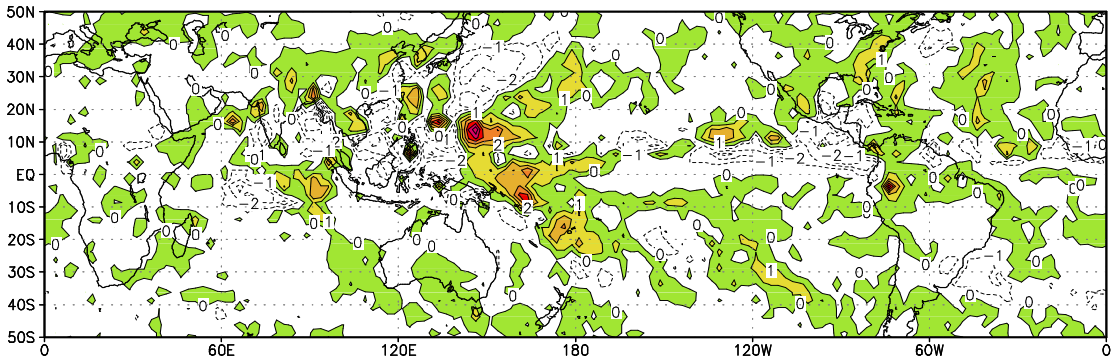

(b)

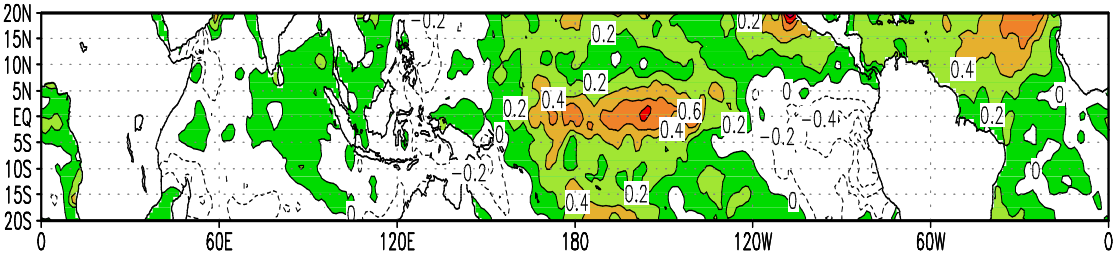

Figure 1 Anomalous conditions during JJAS 2004 (a) for rainfall in cm/month (b) SST in ºC. The datasets of Version 2 Global Precipitation Climatology Project Monthly Precipitation Analysis [*Adler et al.*, 2003], and the Hadley Centre Global Sea Ice and Sea Surface Temperature (HadISST) Analyses [*Rayner et al.,* 2003] for the period 1979-2004 were used to obtain Figures 1a and 1b respectively.

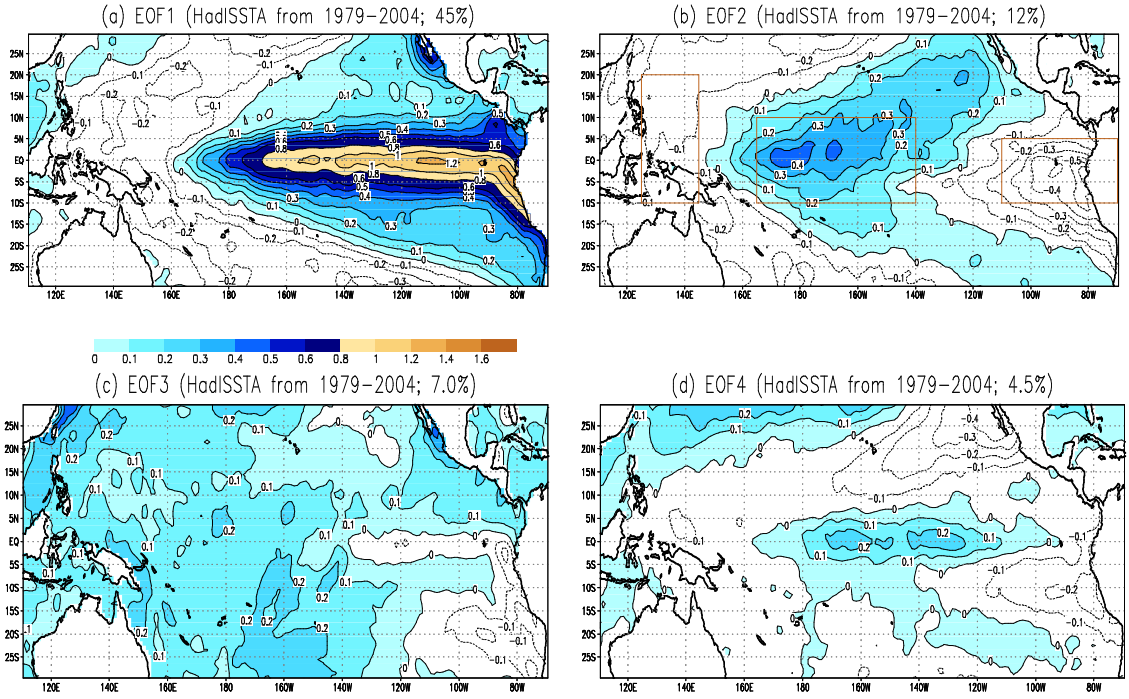

Figure 2 Top four EOF modes of tropical Pacific SSTA (1979-2004) multiplied by respective standard deviations of the principal components; units in ºC.

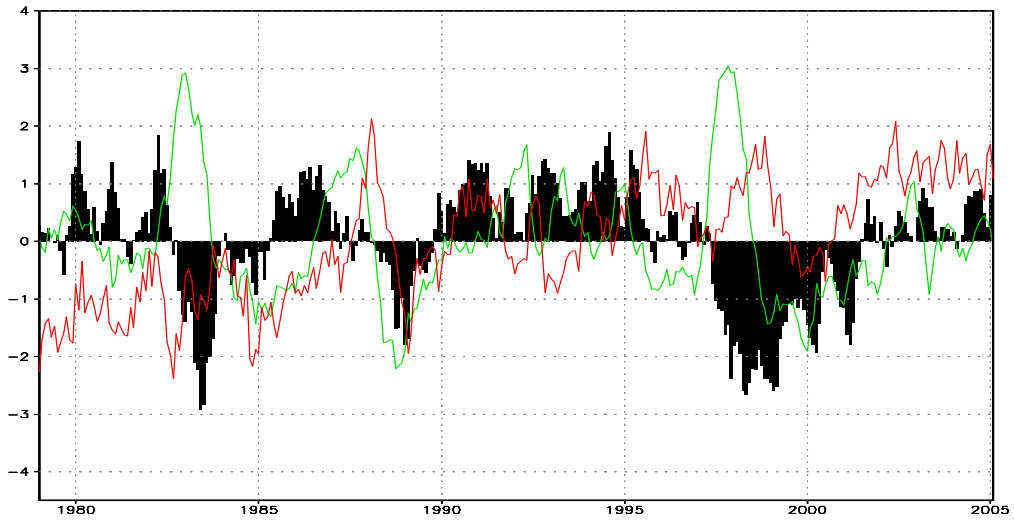

Figure 3 Normalized time series of PC1 (green line), PC2 (bar), and PC3 (red line).

(a)

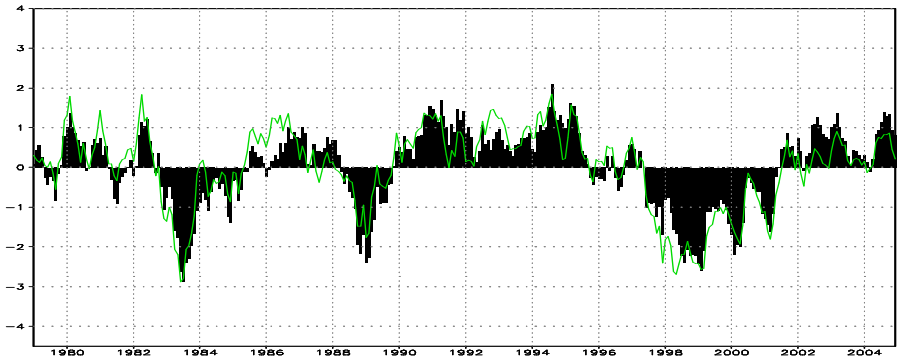

(b)

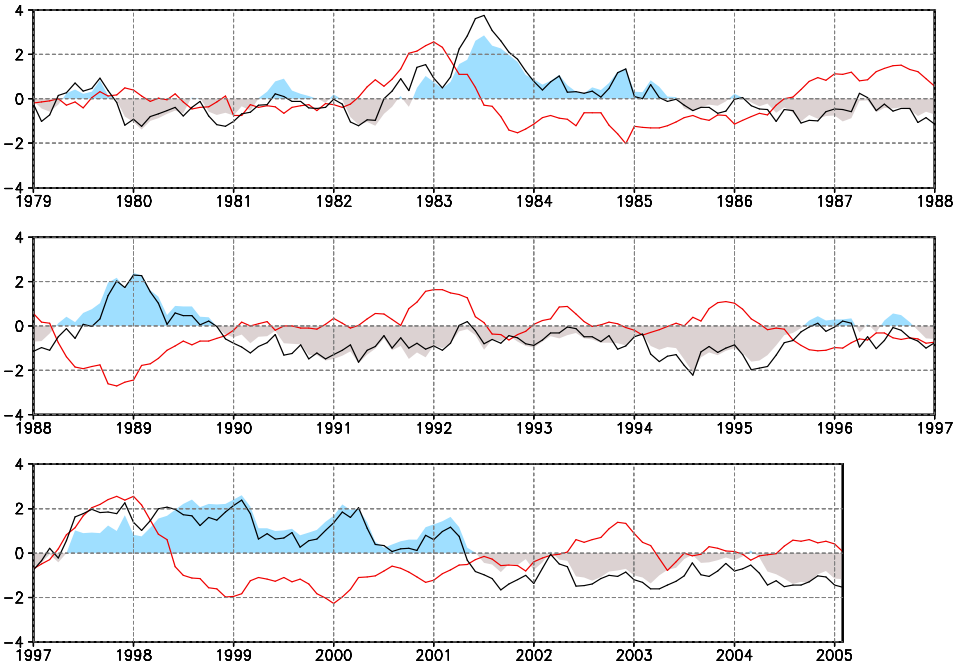

Figure 4 (a) Time series of normalized ENSO Modoki index (EMI; in bar) and that of the PC2 (thin line). The standard deviation of the EMI is 0.52ºC. (b) The time series of Nino3.4 (red line) index, and TNI (blue line) as defined by Trenberth and Stepaniak (2001). Also shown is the time series of the *inverted* EMI (shaded). The sign of the EMI has been deliberately reversed in this figure to facilitate easy comparison of its evolution with the TNI.

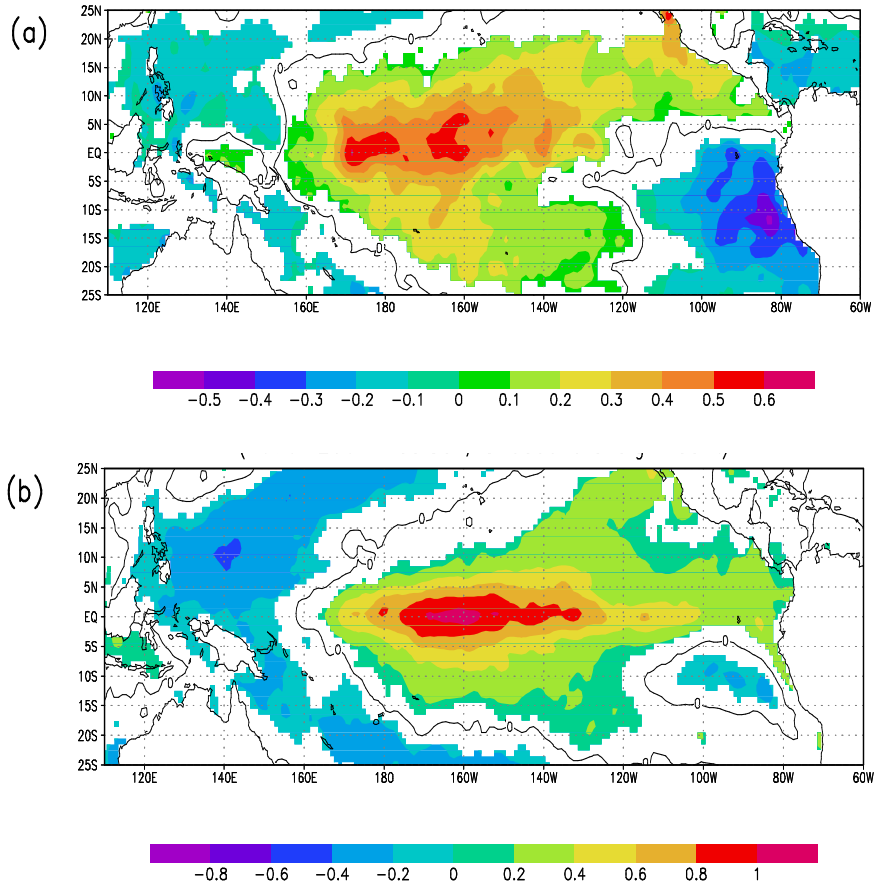

Figure 5 Composite SSTA in ºC during strong positive El Niño Modoki events averaged over (a) seven boreal summers, namely JJAS seasons of 1986,1990, 1991, 1992, 1994, 2002 and 2004 and (b) 8 boreal winters, namely DJF seasons of 1979-80, 1986-87,1990-91, 1991-92, 1992-93, 1994-95, 2002-2003 and 2004-05. Significant values above 95% confidence level from a two tailed Student's t-test are shaded.

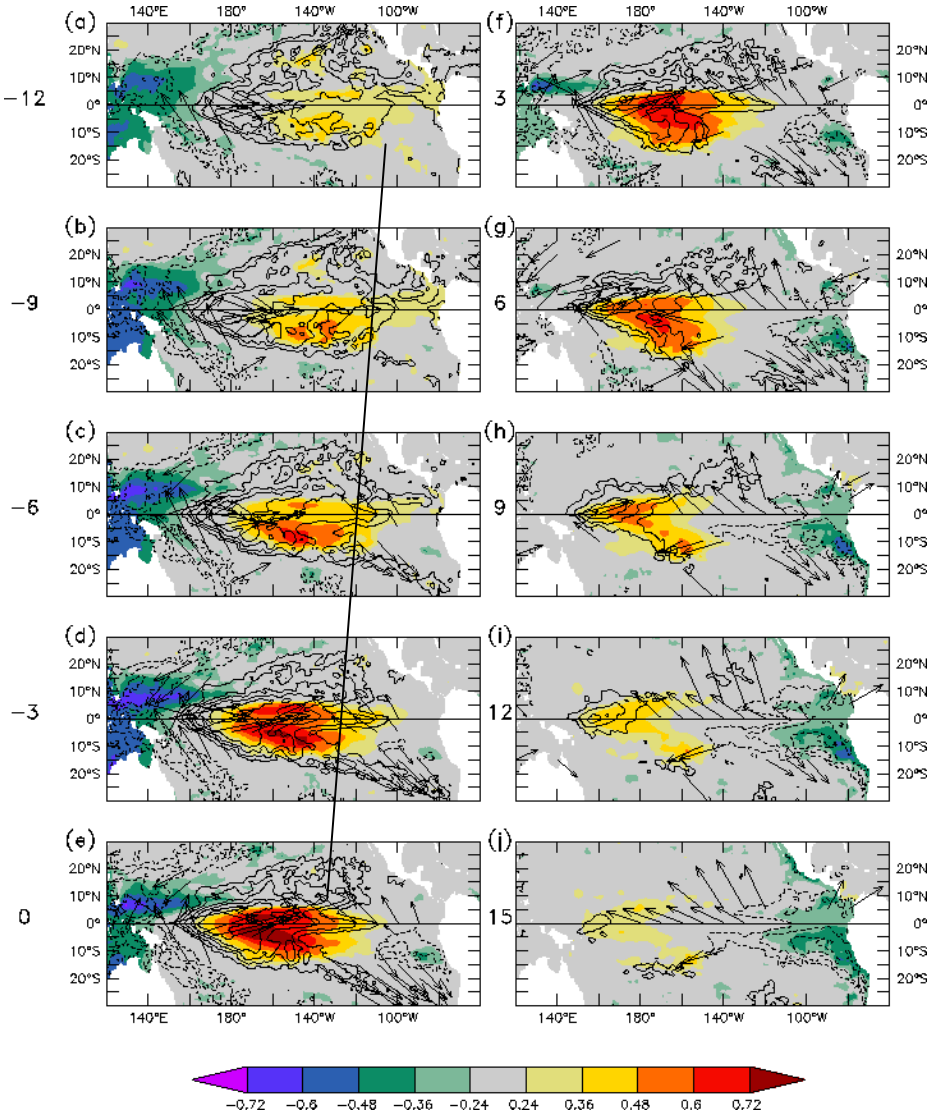

Figure 6 Lag/lead correlations of monthly EMI with sea surface height anomalies (shading) and ocean temperature anomalies at 10 meter depth (contours). Positive (negative) correlation coefficients correspond to high (low) of sea level anomalies. Regressed winds with EMI are shown only if the correlation coefficient between EMI and respective wind components exceeds 0.24; significant correlations at a 80 % (90%) confidence level are 0.24 (0.3) from a 2-tailed Student's t-test after taking into account the autocorrelations of EMI). The positive (negative) numbers to the left of each panel indicate the months by which the EMI leads (lags) the anomaly distribution fields. The thin line extending from (b) to (e) side indicates the propagation of off-equatorial Rossby waves.

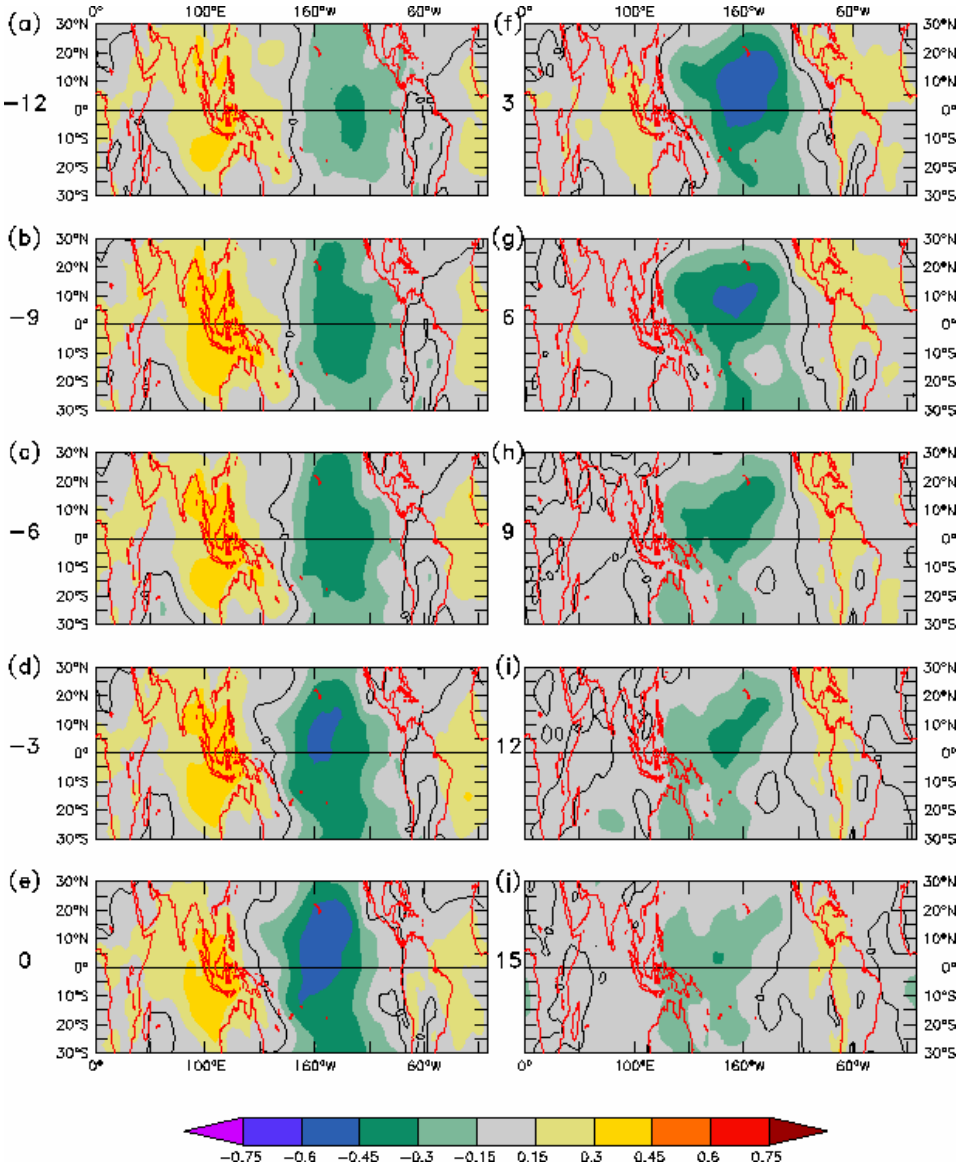

Figure 7 Lag/lead correlations of monthly EMI with sea level pressure anomalies. The positive (negative) numbers to the left of each panel indicate the months by which the EMI leads (lags) the anomaly distribution fields.

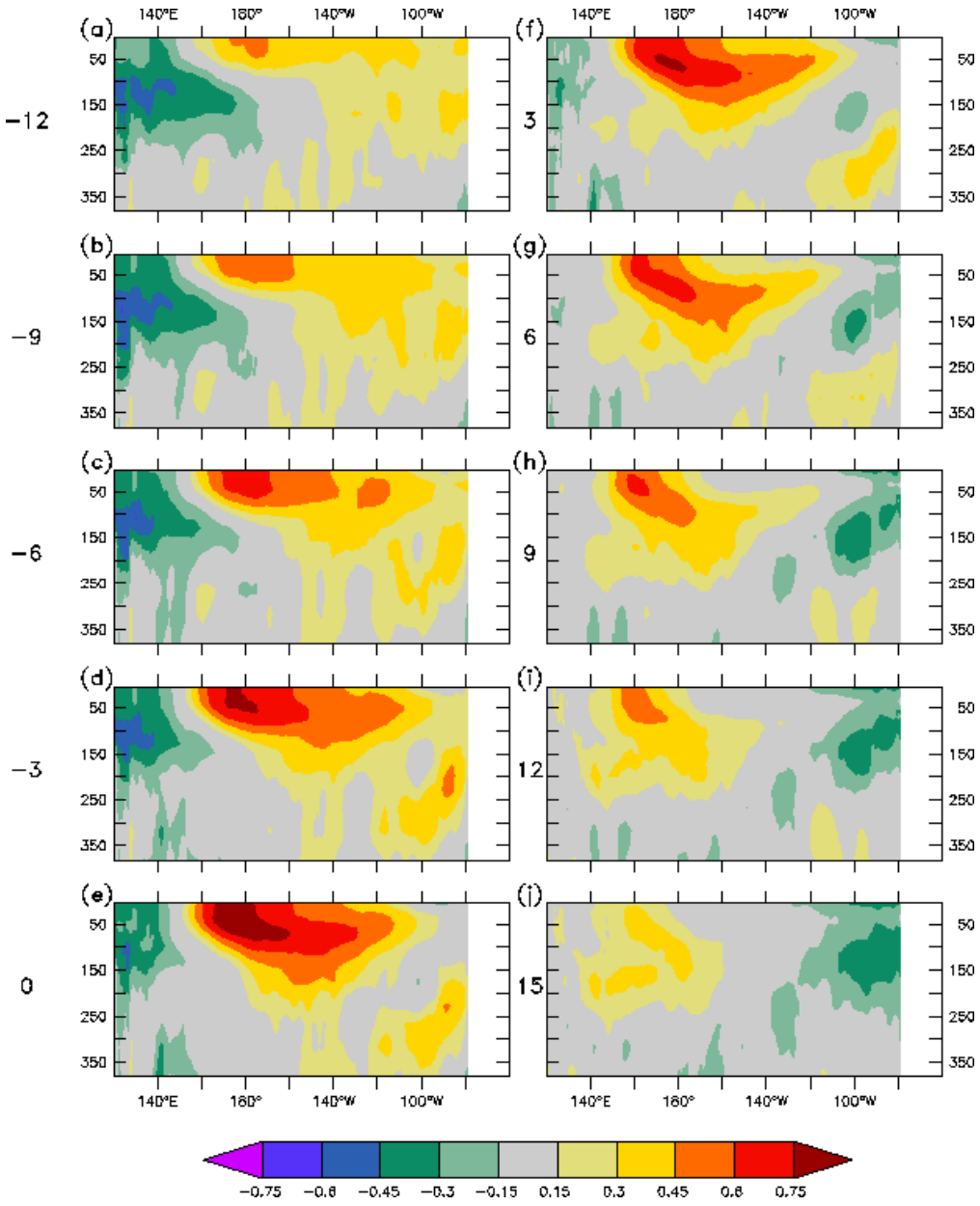

Figure 8 Lag/lead correlations of EMI with ocean subsurface temperature anomalies at different depths in meters averaged over 2°S-4°S. The positive (negative) numbers to the left of each panel indicate the months by which the EMI leads (lags) the anomaly distribution fields.

(a)

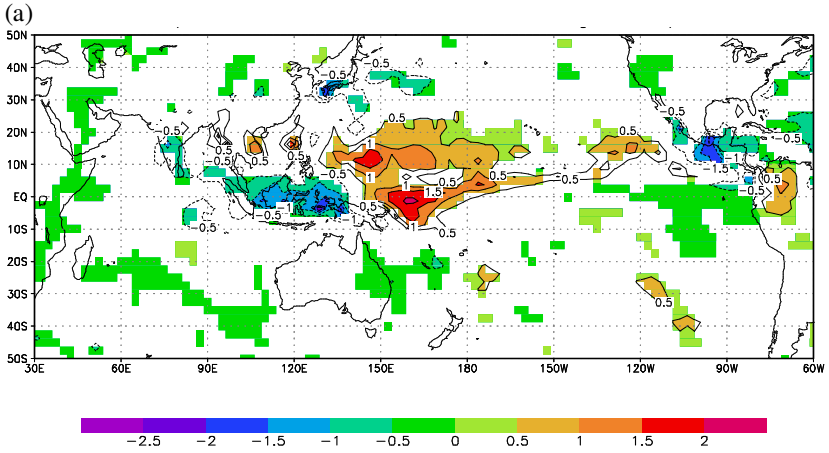
50N
40N
30N
20N
10N
EQ
10S
20S
30S
40S
50S
30E
60E
90E
120E
150E
180
150W
120W
90W
60W
−2.5 −2 −1.5 −1 −0.5 0 0.5 1 1.5 2

(b)

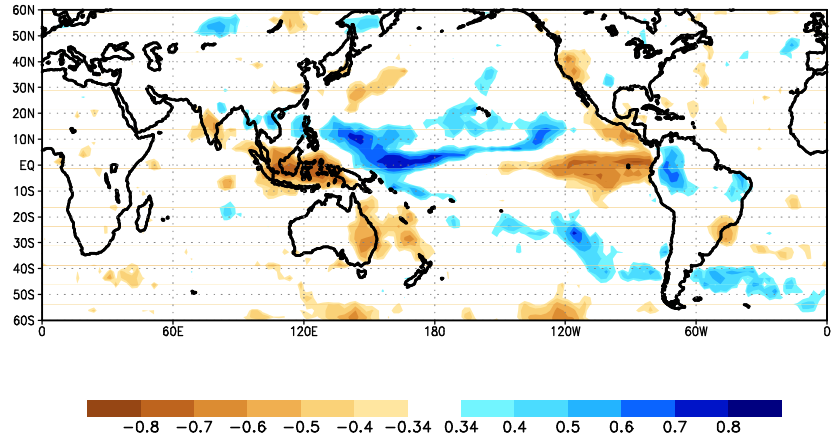
60N
50N
40N
30N
20N
10N
EQ
10S
20S
30S
40S
50S
60S
0
60E
120E
180
120W
60W
0
−0.8 −0.7 −0.6 −0.5 −0.4 −0.34 0.34 0.4 0.5 0.6 0.7 0.8

(c)

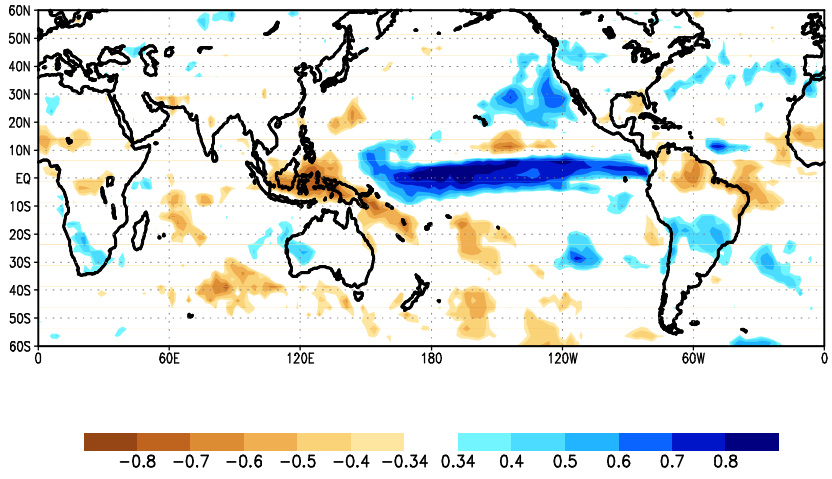
60N
50N
40N
30N
20N
10N
EQ
10S
20S
30S
40S
50S
60S
0
60E
120E
180
120W
60W
0
−0.8 −0.7 −0.6 −0.5 −0.4 −0.34 0.34 0.4 0.5 0.6 0.7 0.8

(d)

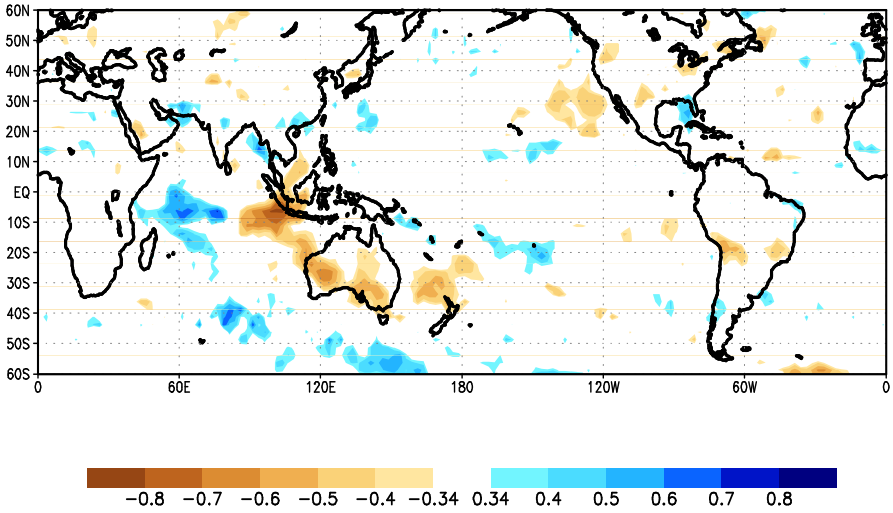

Figure 9 (a) Composite JJAS GPCP rainfall anomalies (cm/month) during strong positive El Niño Modoki events averaged over seven boreal summers, namely JJAS seasons of 1986,1990, 1991, 1992, 1994, 2002 and 2004. (b) JJAS (1979-2004) partial correlations of GPCP rainfall anomalies with EMI. shaded regions are significant at 90% confidence level from a 2-tailed Student's t-test. See text for details. (c) Same as (b) but with NINO3 index. (d) Same as (b) but with IODMI.

(a)

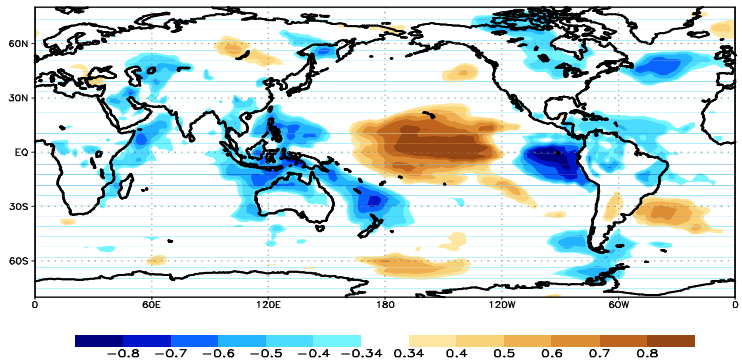

(b)

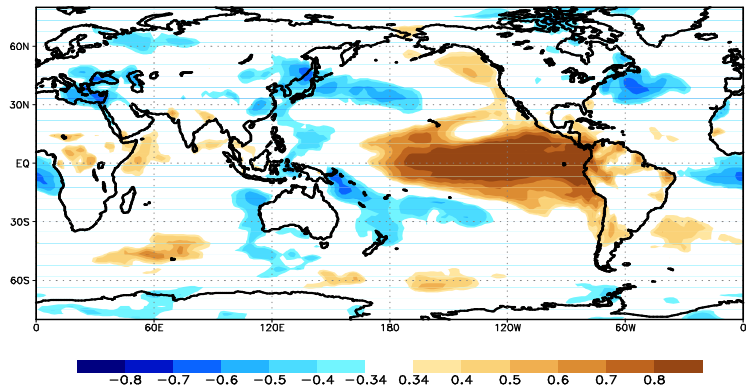

(c)

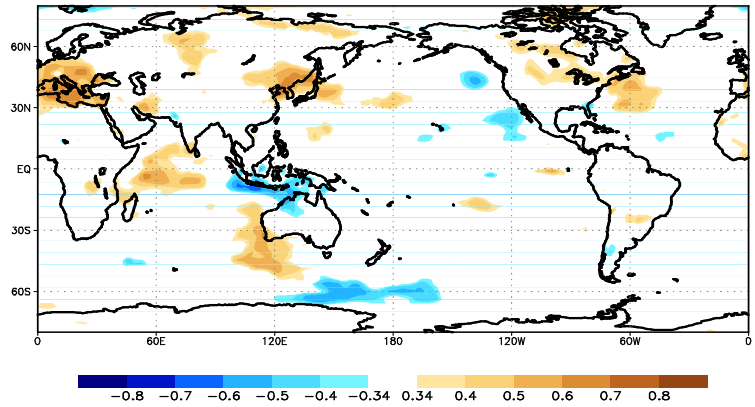

Figure 10 (a) JJAS (1979-2004) partial correlations between temperature (2m height) anomalies and EMI. (b) JJAS (1979-2004) partial correlations between temperature (2m height) anomalies and NINO3 index. (c) JJAS (1979-2004) partial correlations between temperature (2m height) anomalies and IODMI. Shaded values are significant at 90% confidence level from a two tailed Student's t-test.

(a)

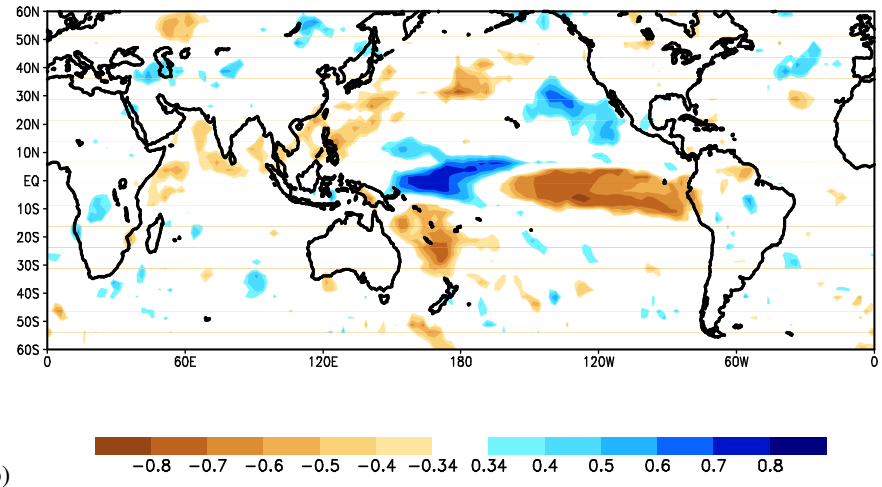

(b)

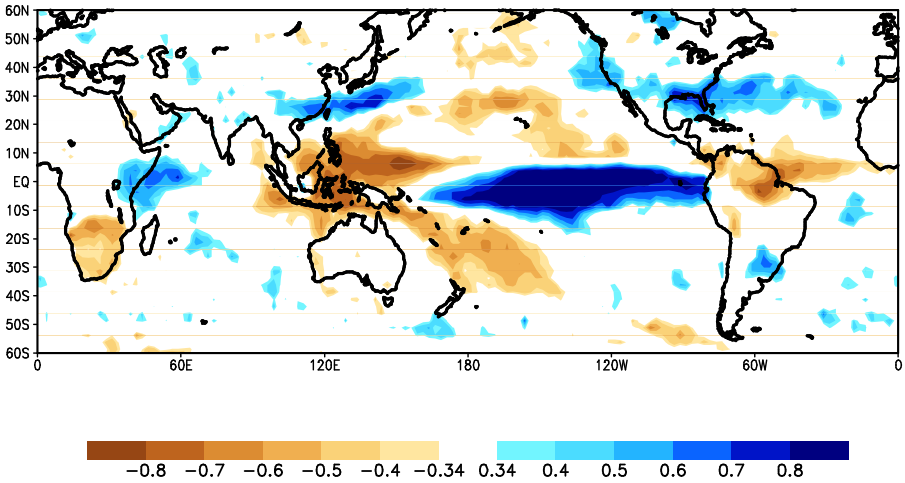

Figure 11 (a) DJF (1979-2004) partial correlations between GPCP rainfall anomalies and EMI. Shaded values are significant at 90% confidence level from a two tailed Student's t-test. (b) DJF (1979-2004) partial correlations between GPCP rainfall anomalies and NINO3 index. Shaded values are significant at 90% confidence level from a two tailed Student's t-test.

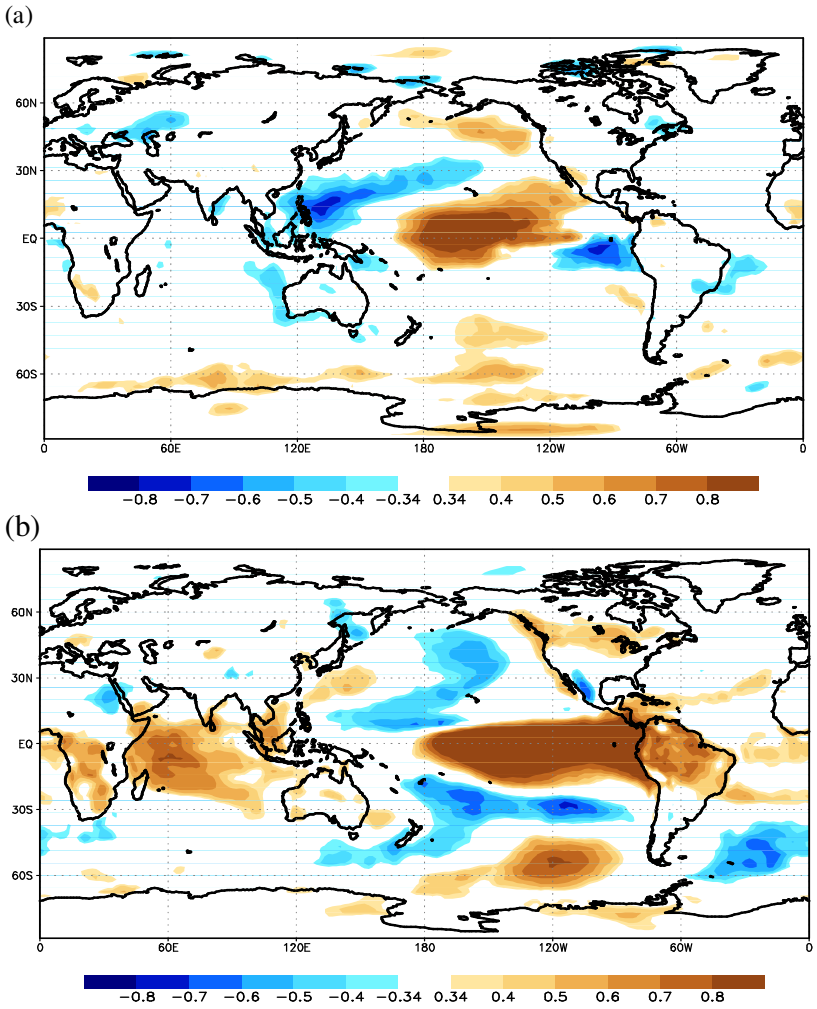

Figure 12 (a) DJF (1979-2004) partial correlations between temperature (2m height) anomalies and EMI. (b) DJF (1979-2004) partial correlations between temperature (2m height) anomalies and NINO3 index. Shaded values are significant at 90% confidence level from a two tailed Student's t-test.

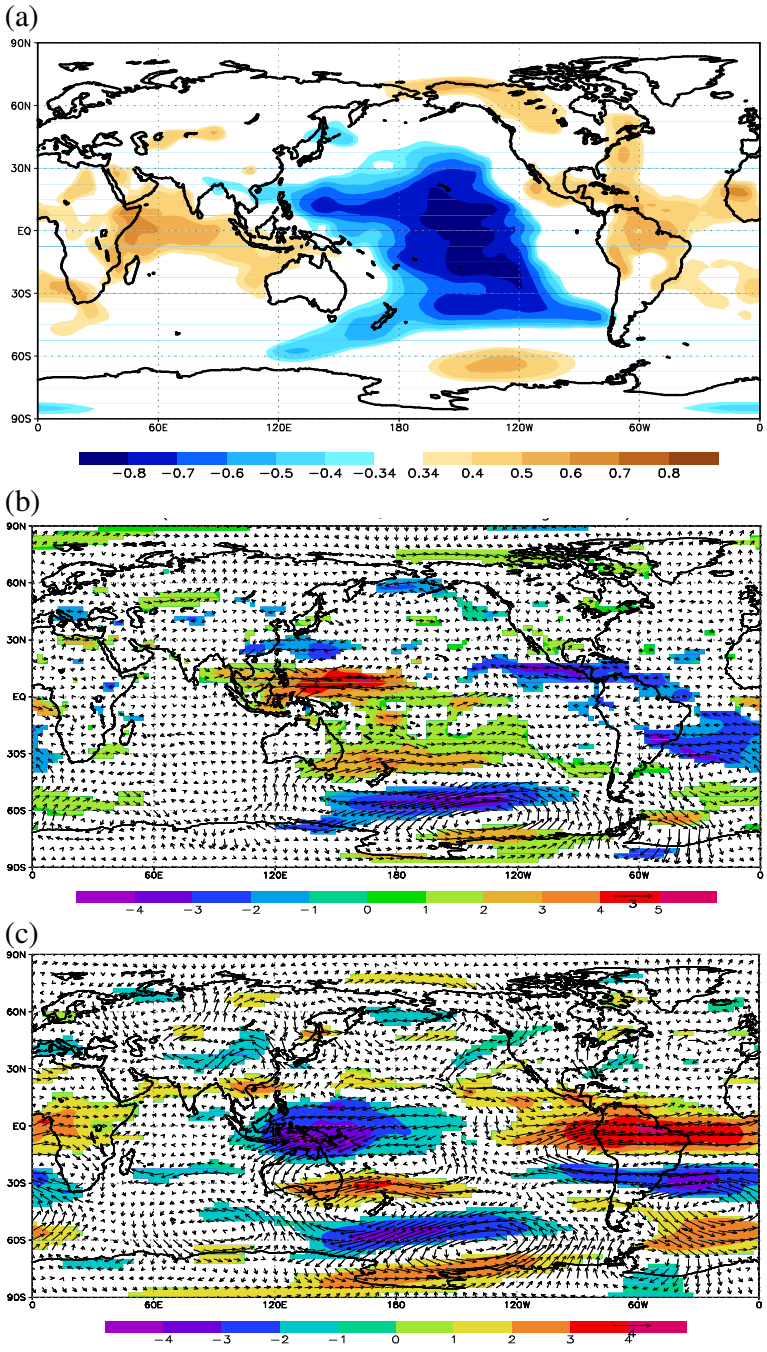

Figure 13 (a) JJAS (1979-2004) partial correlations between SLPA and EMI. (b) Composite JJAS 850 hPa anomalous winds obtained from seven strong El Niño Modoki events. (c) Same as (b) but at 200 hPa level. Shaded values are significant at 90% confidence level from a two tailed Student's t-test

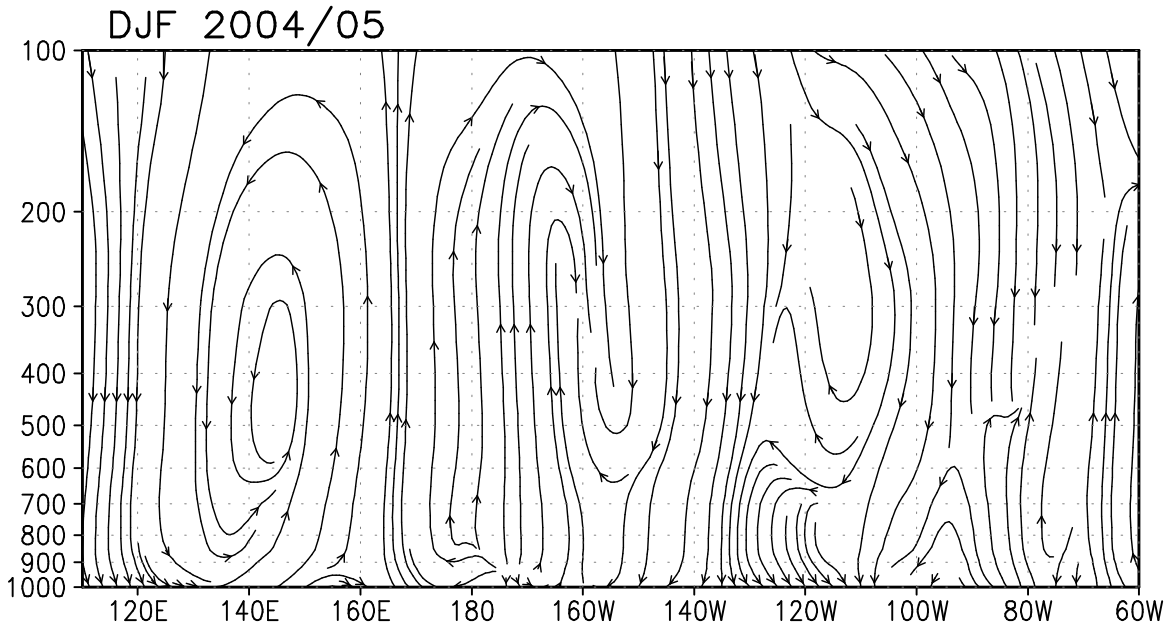

Figure14 2004/05 DJF anomalous Walker circulation streamlines averaged from 10ºS to 10ºN.

(a)

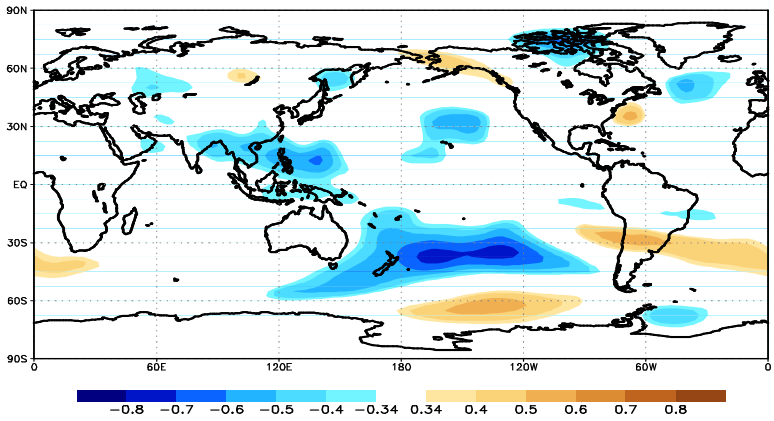

(b)

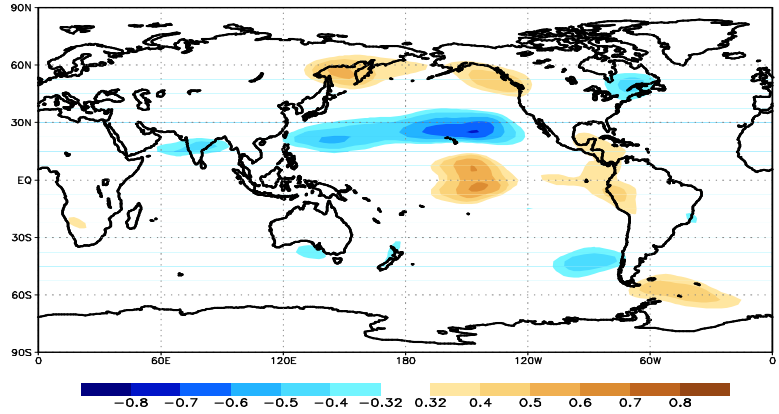

Figure 15 (a) JJAS (1979-2004) partial correlations between 500 hPa geopotential anomalies and EMI. Shaded values are significant at 90% confidence level from a two tailed Student's t-test. (b) Same as Figure 15(a) but during DJF (1979-2004).

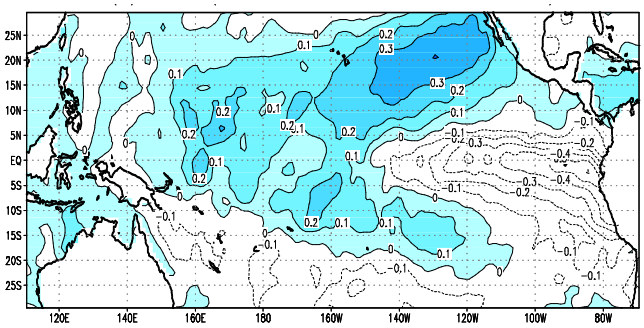

Figure 16 EOF2 mode of tropical Pacific SSTA (1958-1978) multiplied by the standard deviation of its principal component; units in ºC. This mode explains about 10% of the tropical Pacific SSTA variance.

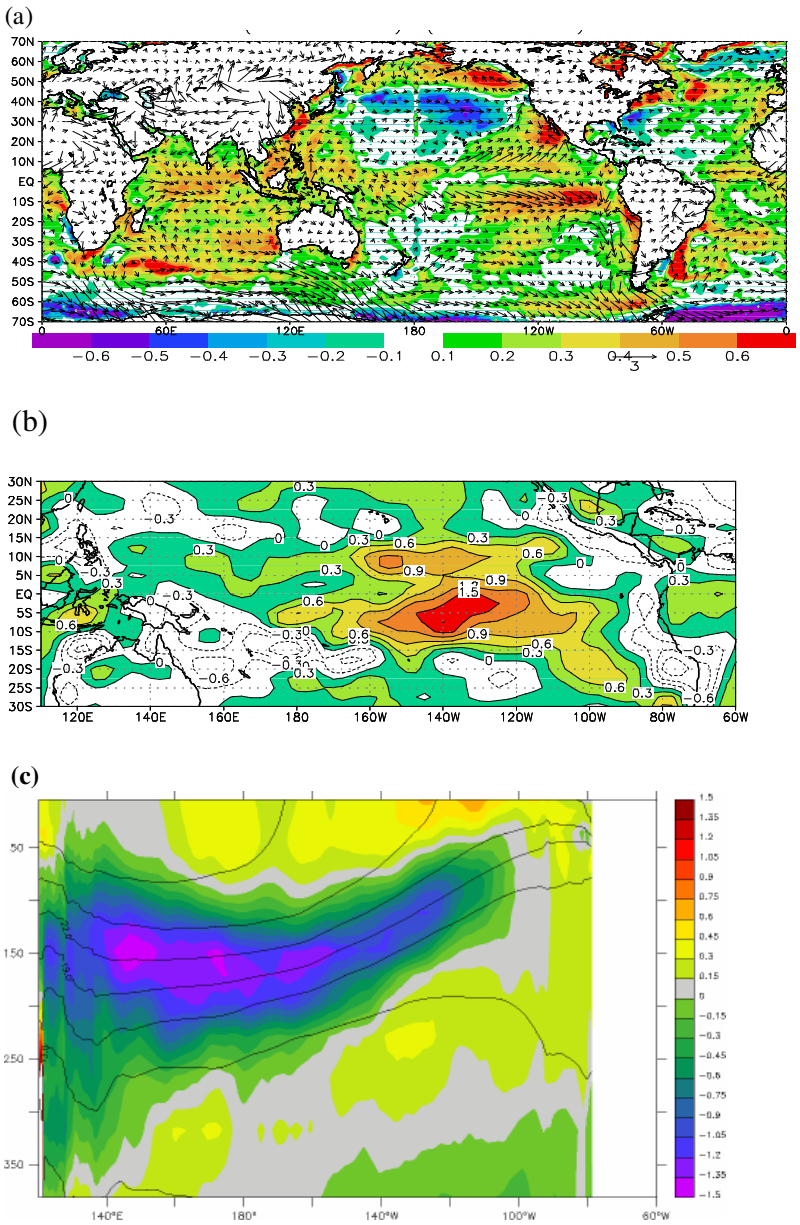

Figure 17 (a) Long-term changes in mean SST (ºC) and winds at 1000 hPa (m/s), obtained by subtracting the mean SST of the period 1958-1978 from that over the period 1979-2004. (b) Long term changes in annual mean zonal winds at 1000 hPa (m/s), obtained as in (a). (c) Differences of ocean temperature in two periods of 1958-78 and 1978-2004 along with the depth-longitude section of climatological ocean temperature (black contours).

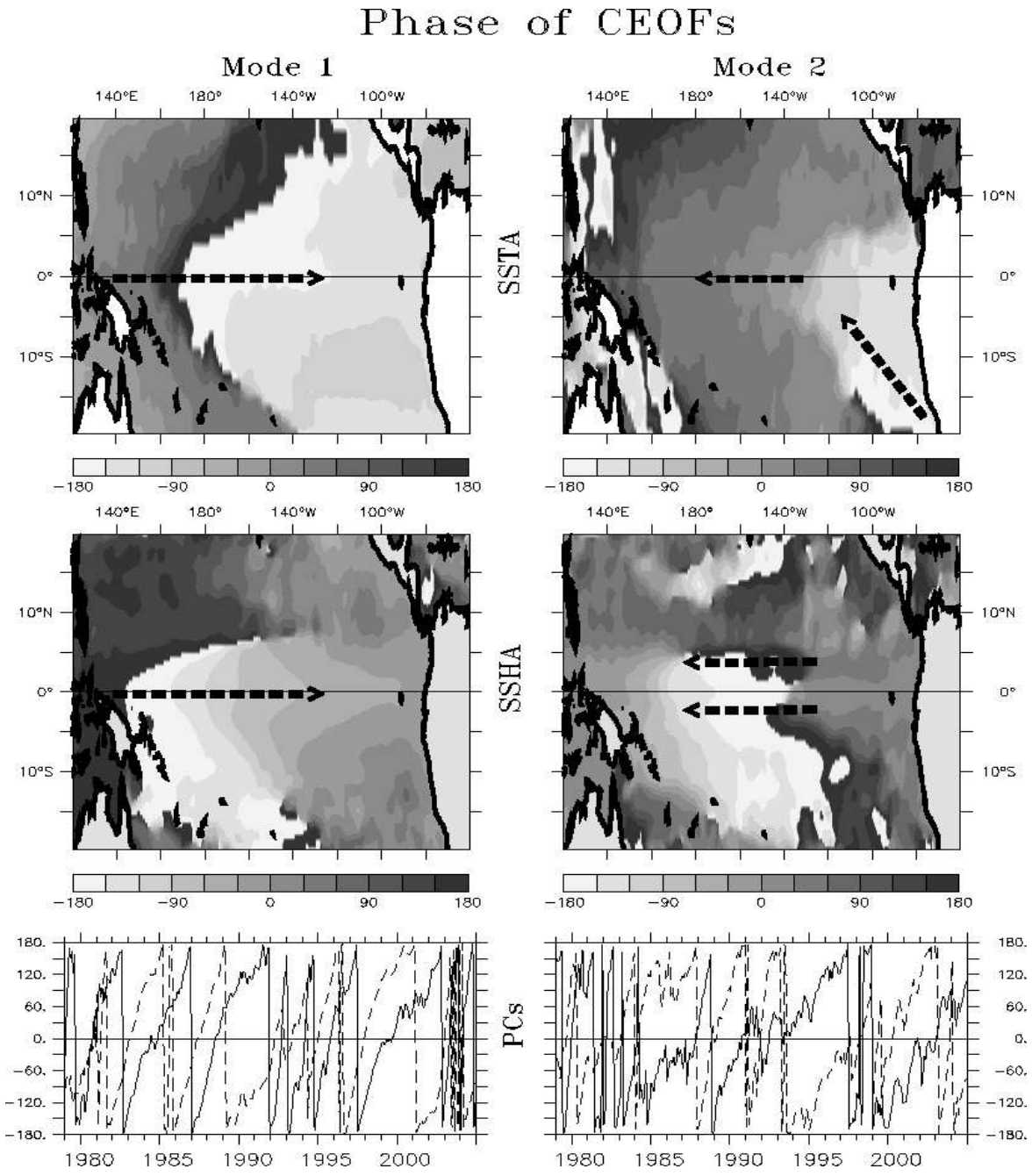

Figure A1-1: The phase information of complex EOF1 (top left) and complex EOF2 (top right) of SSTA. Similar information for SSHA is provided in the middle panels. The bottom panels provide the respective principal components, with thick (dashed) lines representing the SSTA (SSHA).

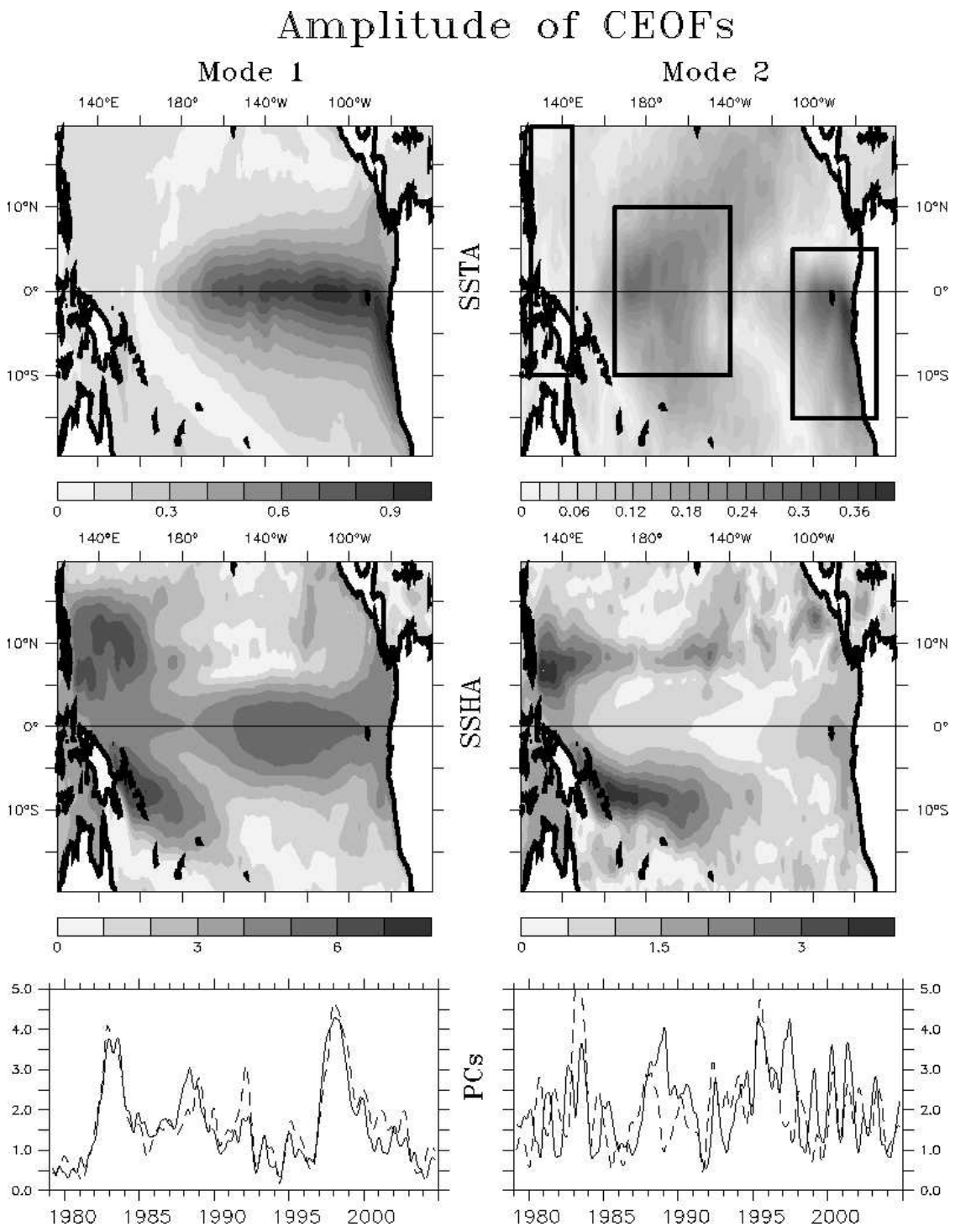

Figure A1-2: The amplitude of complex EOF1 (top left) and complex EOF2 (top right) of SSTA. Similar information for SSHA is provided in the middle panels. The bottom panels provide the respective principal components, with thick lines representing the SSTA and dashed lines for SSHA.

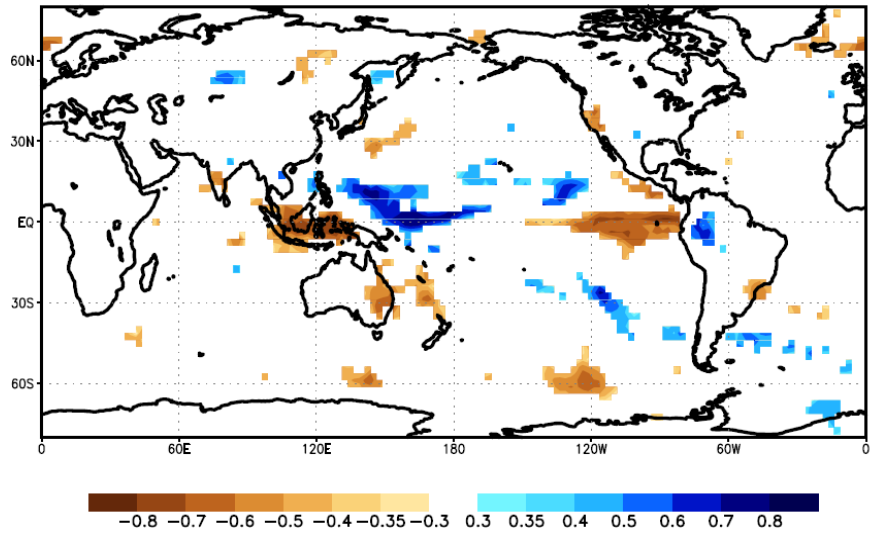

EMI−GPCP (JJAS);other predictors are NINO3 SST & IODMI)

Shaded values are significant at 90% from a Monte−Carlo test with AR(1)

Figure-A2-1

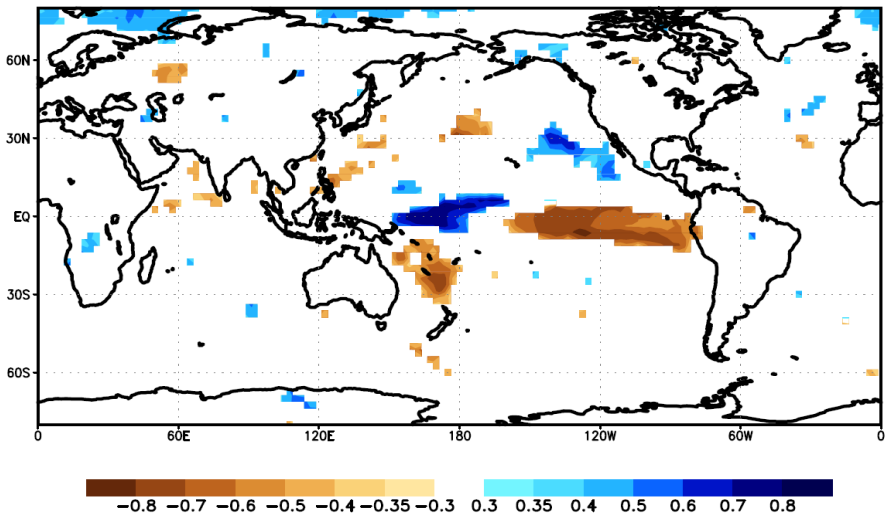

EMI−GPCP (DJF);other predictor isNINO3 SST)

Shaded values are significant at 90% from a Monte−Carlo test with AR(1)

Figure-A2-2